Pool boiling review: Part II – Heat transfer enhancement

M.M. Mahmoud [a], T.G. Karayiannis [b],*

[a] Zagazig University, Faculty of Engineering, Zagazig 44519, Egypt
[b] Brunel University London, Department of Mechanical and Aerospace Engineering, Uxbridge UB8 3PH, UK

A B S T R A C T

Heat transfer enhancement by surface modification has been extensively studied in the last twenty years. However, there remains a large discrepancy among researchers on the performance of enhanced surfaces even for the same fluid and surface preparation technique. The reasons of this discrepancy are not understood and are not discussed in past papers, including paper reviews. Part II of this two-part paper aims to present a detailed assessment of pool boiling heat transfer enhancement, relating this to Part I [1], which presented a critical assessment of fundamental concepts of heterogeneous nucleation. Current challenges in evaluating the performance of enhanced surfaces is first discussed. The performance of smooth and roughened surfaces is then discussed and the effect of fluid type is explained. Pool boiling data of two fluids, namely water and FC-72, on two enhanced substrate materials, i.e. copper and silicon were digitized and assessed in order to elucidate the reason for the discrepancy in published works and present future recommendations for heat transfer enhancement. The heat transfer enhancement mechanisms adopted by researchers were presented and critically discussed and compared. The paper contributes to the understanding of the effect of fluid-surface combinations and suggest guidelines for researchers to consider when evaluating the performance of enhanced surfaces. This will help the research community and industry to conclude on the best surface structure and surface manufacturing technique matching particular fluid of interest.

1. Introduction

Boiling heat transfer enhancement has attracted the focus of researchers in the last twenty years, motivated by the need to improve the heat transfer rates in heat exchangers used in, for example, the power generation, chemical and refrigeration industries where such improvements will result in higher plant efficiencies, reduced size equipment and overall plant size and fluid inventory. The need to achieve high- and ultra-high heat dissipation rates in modern electronics has also added to the stimulus for more research in this area. This is obvious from Fig. 1 that shows the trend in research based on Scopus database with the keywords "boiling" and "enhancement" appearing in the document tittle. It demonstrates that the number of published papers on boiling enhancement increased exponentially in the last years. It is well known that boiling heat transfer rates depend strongly on the number density of active nucleation sites and bubble dynamics (bubble growth rate, departure size and frequency), see Part I [1]. Boiling enhancement techniques are usually classified into either passive or active techniques [2]. Passive techniques include rough, treated surfaces or surfaces coated

with porous structures that increase the number of nucleation sites. Active techniques include surface or fluid vibration, surface rotation or the application of high intensity electric fields. The latter require the use of an external force and are less common than passive heat transfer enhancement techniques. Accordingly, the current paper will focus only on one of the most commonly researched passive enhancement techniques, which is the surface modification by creating micro and/or nanostructures including coatings. The growing interest of researchers with this technique was encouraged by the significant advances in manufacturing techniques that can produce surfaces with a complex structure. One example of these techniques is the additive manufacturing (3D printing), which has the flexibility of fabricating complex geometries. McDonough [3] reviewed and discussed the capabilities of additive manufacturing for process heat transfer applications including the manufacturing methods, technologies and materials. For metal additive manufacturing, three metals were commonly used namely steel/iron-based alloys, titanium/titanium alloys and Inconel/nickel-based alloys. He concluded that although it is very promising, it still faces many challenges such as the control of the surface roughness and post-processing of complex geometries.

Nomenclature

CHF_{enh}	Critical heat flux of the enhanced surface, [W/m^2]
CHF_{ref}	Critical heat flux of the reference surface, [W/m^2]
D	Bubble departure diameter, [m]
E_{HTC}	Enhancement factor in HTC, [–]
E_{CHF}	Enhancement factor in CHF, [–]
f	Bubble generation frequency, [Hz]
g	Acceleration due to gravity, [m/s^2]
$\bar{h}_{q,enh}$	Heat flux-averaged HTC of the enhanced surface, [W/m^2 K]
$\bar{h}_{q,ref}$	Heat flux-averaged HTC of the reference surface, [W/m^2 K]
h_{fg}	Latent heat, [J/kg]
q	Heat flux, [W/m^2]
Q_{site}	Heat transfer rate per nucleation site, [W]
R_a	Arithmetic mean roughness height for a line, [μm]
R_q	Root mean square roughness, [μm]
S_a	Arithmetic mean roughness height for a surface, [μm]
ΔT_{sup}	Wall superheat, [K]

Greek symbols

θ	Contact angle, [deg]
ρ_v	Vapour density, [kg/m^3]

Abbreviations

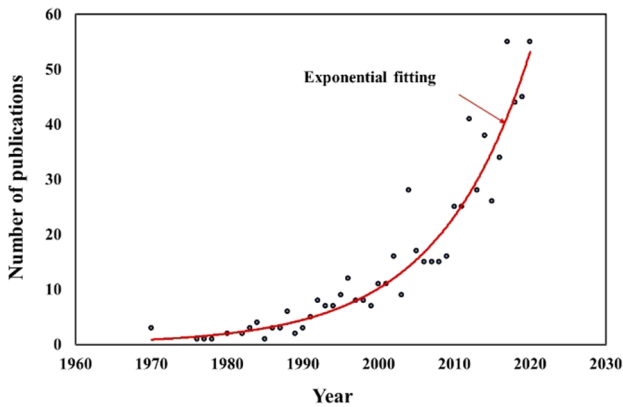|	
CHF	Critical Heat Flux
HTC	Heat Transfer Coefficient
CNC	Computerized Numerical Control
CNT	Carbon Nano Tube
WEDM	Wire Electric Discharge Machining
PTFE	Polytetrafluoroethylene

Fig. 1. The trend in research on boiling heat transfer enhancement – based on a search in Scopus database.

A review of the past reports reveals that there is still a large discrepancy among researchers on the performance of enhanced surfaces for the same fluid and enhancement technique, despite the large number of researches conducted in this area. The reasons of this discrepancy are not understood and were not discussed in the past review papers. In most studies, the boiling surface was designed randomly without adopting any design criteria with the sole purpose of increasing the number of nucleation sites on the surface. The question of an upper limit in the increase of the number of nucleation sites on a surface arises. This is due to the fact that when one nucleation site becomes active, it may suppress some of the surrounding nucleation sites in the area of bubble influence. Designing the surface randomly and ignoring fundamental theories of heterogeneous nucleation and bubble dynamics may be one of the reasons of discrepancy among researchers. In Part I [1], the fundamentals of boiling surface design (heterogeneous nucleation and bubble dynamics) were presented and discussed to help understand the performance of enhanced surfaces discussed in the present Part II paper.

In the past review papers there was no segregation to the fluid-surface combination and instead various fluids and various surface modification techniques were included in the discussion. This approach makes it difficult to understand the performance of a certain fluid on a wide range of surface microstructures. Accordingly, in the present paper, the focus was on the boiling performance of two fluids (water and FC-72) and two commonly tested substrate materials (copper and silicon). Water was selected to represent liquids with high surface tension, high latent heat and moderate wetting, while FC-72 was selected to represent liquids with low surface tension, low latent heat and high

wetting. With this approach, it will be possible to compare the existing studies against each other for a given fluid and surface modification approach. This will help understand the effect of fluid-surface combination. The paper discusses only the boiling performance of horizontal upward facing flat surfaces with pure liquids at atmospheric pressure. It is worth mentioning that the performance of other fluids such as cryogenic liquids, refrigerants and hydrocarbons are not included in this paper so as to make the paper focused and conclusive.

2. Boiling performance of enhanced surfaces

In this section, a comparison between the boiling heat transfer performance of enhanced surfaces is presented and discussed. To have a fair comparison, the following rules were adopted: (i) the data (heat flux versus superheat) of the best performing surface in each study were extracted from the published figures, (ii) the enhancement factor in HTC was calculated based on the heat flux-averaged heat transfer coefficient ($\bar{h}_q$) as follows:

$$\bar{h}_q = \frac{1}{q_f - q_i} \int_{q_i}^{q_f} h(q)\,dq \tag{1}$$

where q_i and q_f are the first and last recorded heat flux values in each study. In literature, the enhancement factor was reported based on the maximum HTC (at one heat flux value), which in some cases occurs at very low heat fluxes. Thus, inferring the performance of the surface based on one heat flux value may not be accurate. Because the definition of the best performing surface is subjective, the best surface will be defined in the current discussion as the one that achieves high enhancement factors in HTC and CHF. In several studies, a number of surfaces was tested and some surfaces achieve high CHF but low HTC compared to other surfaces. Thus, when the difference in CHF between two surfaces is less than 10 %, the surface with lower superheat (higher heat transfer rate) will be considered in our discussion as the best performing surface. In most studies, the experimental uncertainty in the measured heat flux is less than 10 % (about 8 % in most cases). In other words, a compromise between CHF and HTC will be conducted in the extracted data analysis. It is worth mentioning that the calculated enhancement factors in CHF and HTC in our discussion may differ from the reported enhancement factors in the original published papers. From now on in this paper, HTC means the heat-flux averaged heat transfer coefficient (eq. (1)). And the enhancement ratio in the heat transfer coefficient and critical heat flux are given as:

$$E_{HTC} = \frac{\bar{h}_{q,enh}}{\bar{h}_{q,ref}} \tag{2}$$

and

$$E_{CHF} = \frac{CHF_{enh}}{CHF_{ref}} \tag{3}$$

where $\bar{h}_{q,enh}$ is the heat flux-averaged heat transfer coefficient of the enhanced surface, $\bar{h}_{q,ref}$ is the heat flux-averaged heat transfer coefficient of the reference surface, CHF_{enh} is the critical heat flux of the enhanced surface, and CHF_{ref} is the critical heat flus of the reference surface. Before discussing the performance of enhanced surfaces, it is important to start with understanding the performance of the reference smooth and roughened surfaces. In all studies, the HTC was calculated as: $HTC = q/\Delta T_{sup}$. The heat flux was based on the projected are not the actual area of the enhanced surface.

2.1. Smooth surfaces

Table 1 lists the performance of the reference surface reported in previous studies, which includes different substrate materials and fluids.

The following points can be concluded from Table 1: (i) For water–silicon, there is no agreement on the measured CHF (0.7–1.5 MW/m²) and there is a difference in the HTC (15–22 kW/m² K). (ii) For water-metals, there is a wide scatter in the HTC and CHF. For example, the HTC on copper substrates ranged from 19.6 kW/m² K to 72.3 kW/m² K and the CHF value ranged from 0.8 to 1.6 MW/m². For water-aluminum, the HTC ranged from 28 to 40 kW/m² K and the CHF ranged from 1.3 to 1.8 MW/m². For water-stainless steel, the HTC ranged from 16 to 46 kW/m²K and the CHF was about 0.9 MW/m². This large variation could be due to differences in the surface microstructure of the plain surface, which indicates that there is no standard definition to what is called "smooth surface". Without standard definition to the smooth surface, the reported enhancement factors in literature may be misleading, e.g. a comparison with an extremely smooth reference surfaces may lead to large values of enhancement factors. Additionally, there is no general criterion to infer the onset of the CHF. The commonly adopted criterion by nearly all researchers was the rise in wall superheat by a certain value. If one researcher allowed for 10 K rise in superheat between two consecutive heat flux steps and someone else allowed for 20 K, the CHF
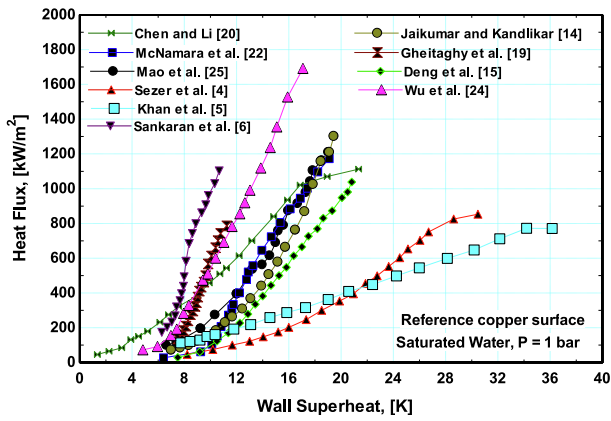
Table 1
Heat transfer performance of plain smooth surfaces.

Author	Fluid	Material	Surface preparation	Roughness value, [μm]	θ, [deg]	HTC, [kW/m²K]	CHF, [MW/m²]	ΔT_{CHF} [K]
Kim et al. [7]	Water	Si	Not reported	0.00175	44.6	18.1	0.993	35.9
Liu et al. [8]	Water	Si	Not reported	Not reported	–	21.8	0.98	28.3
Liu et al. [9]	Water	Si	Not reported	Not reported	–	11.9	0.7	45
Yao et al. [10]	Water	Si	Not reported	Not reported	–	14.5	0.72	43
Kwak et al. [11]	Water	Si	Not reported	Not reported	60.2	21	1.5	47
Lim and Bang [12]	Water	Si	Not reported	Not reported	41.8	15.2	0.8	36
Rioux et al. [13]	Water	Cu	Not reported	Ra = 0.068	73.3	38.3	1.24	21.3
Jaikumar and Kandlikar [14]	Water	Cu	Not reported	Not reported	–	41.8	1.3	19.45
Deng et al. [15]	Water	Cu	EDM	R_q = 2.9	–	31.75	1.04	20.8
Sankaran et al. [6]	Water	Cu	Not reported	Not reported	70	72.1	1.1	10.7
Souza et al. [16]	Water	Cu	Abrasive aluminum oxide	R_q = 0.05	95	30.9	0.772	17.1
Sezer et al. [4]	Water	Cu	Not reported	Not reported	74	19.74	0.853	30.5
Kumar et al. [17]	Water	Cu	Not reported	R_q = 0.05	58	72.3	1.25	11.3
Rishi et al. [18]	Water	Cu	Not reported	Not reported	–	37.8	1.23	24
Gheitaghy et al. [19]	Water	Cu	Sandpaper	R_q = 0.2	70	51.8	0.85	13.9
Chen and Li [20]	Water	Cu	Not reported	Not reported	69.7	47.9	1.11	21.3
Gupta and Misra [21]	Water	Cu	Emery paper Grit 2000	R_q = 0.2	65	38.8	1.06	20.1
MacNamara et al. [22]	Water	Cu	CNC machining	R_q = 0.25	84	40	1.18	19.1
Kruse et al. [23]	Water	Cu	Not reported	Not reported	–	45.74	1.7	23.9
Khan et al. [5]	Water	Cu	Not reported	Not reported	74	19.6	0.771	36.2
Wu et al. [24]	Water	Cu	CNC	Not reported	–	61.1	1.7	17.1
Mao et al. [25]	Water	Cu	Not reported	Not reported	89.3	43.3	1.21	19
Kim et al. [26]	Water	Al	Sandpaper Grit 2000	R_a = 0.11	12.4	28.4	1.6	43.16
Hayes et al. [27]	Water	Al	Not reported	Not reported	–	43.1	1.26	23.5
Godinez et al. [28]	Water	Al	Sandpaper Grit 600	Not reported	12	39.8	1.822	30.96
Kruse et al. [29]	Water	SS	Not reported	Not reported	80	15.52	0.9	40
Zhang et al. [30]	Water	SS	Not reported	Not reported	–	45.8	0.86	12.3
Ujereh et al. [31]	FC-72	Si	Not reported	Not reported	–	2.1	0.112	34
Liu et al. [32]	FC-72	Si	Not reported	Not reported	–	3.39	0.165	36.2
Zhou et al. [33]	FC-72	Si	Not reported	Not reported	–	3.02	0.154	32.1
Duan et al. [34]	FC-72	Si	Not reported	Not reported	–	3.95	0.158	29.7
Lei et al. [35]	FC-72	Si	Not reported	Not reported	–	3.22	0.163	36.3
Yu and Lu [36]	FC-72	Cu	EDM machining	Not reported	–	5.04	0.178	26.9
Ujereh et al. [31]	FC-72	Cu	Sandpaper	Not reported	–	7.3	0.168	20.8
Kumar et al. [37]	FC-72	Cu	Emery paper – unspecified	Not reported	15	2.84	0.153	34.9
Sarangi et al. [38]	FC-72	Cu	Diamond sheet polishing	Not reported	–	2.76	0.113	27.9
Kumar et al. [39]	FC-72	Cu	Mechanical and chemical polishing	Not reported	5	3.39	0.181	35.8
Zimmermann et al. [40]	FC-72	Cu	Not reported	S_a = 0.627	15.6	7.85	0.159	11.9
Kim et al. [41]	FC-72	Al	Alumina compound	R_q = 0.09	15.9	3.85	0.159	31.6
McHale et al. [42]	HFE-7300	Cu	Mill-grade finish	Not reported	–	4.77	0.173	22.9
Wu et al. [43]	HFE-7200	Cu	Emery paper Grit 2000	R_a = 0.1	24.4	3.6	0.191	39.6
Cao et al. [44]	HFE-7200	Cu	Emery paper Grit 2000	R_a = 0.085	22.6	3.62	0.192	39.6
Doran et al. [45]	HFE-7100	Al	Sandpaper Grit size 1200	Not reported	5	3.26	0.127	46.3

Fig. 2. Saturated boiling of water on the reference copper surface in each study.

value is expected to be different. Fig. 2 depicts the boiling curve for saturated boiling of water at atmospheric pressure on a copper reference surface. As seen in the figure, all surfaces do not agree with each other and the reference surface by Sezer et al. [4] and Khan et al. [5] seems to be extremely smooth while that tested by Sankaran et al. [6] seems to be extremely rough.

From Table 1, the effect of fluid properties can be explained through a comparison between water and FC-72 on silicon substrates. Silicon substrate was selected because it is expected to have minor differences in surface microstructure. This comparison is shown in Fig. 3 at atmospheric pressure including two studies for each fluid. The following points can be concluded from this figure:

(i) For water, boiling starts at much lower wall superheat (8–12 K) compared to FC-72 which occurred at about 39–47 K with an obvious temperature excursion. It is interesting to note that, this contradicts the prediction using the simple equilibrium superheat equation (Eq. (2) in Part I [1]). It predicts that the incipience superheat of water must be larger than that of FC-72 due to the large surface tension of water (more than seven times larger than FC-72), see the discussion of Fig. 12 in Part I, [1]. For example, with a fixed cavity radius of about 0.1 μm (assumed for silicon), the predicted incipience superheat will be about 329 K for water and about 48 K for FC-72. A similar behavior with the possible explanation was reported and discussed in Part I for boiling water and ethanol on sapphire substrate. Some possible reasons of the
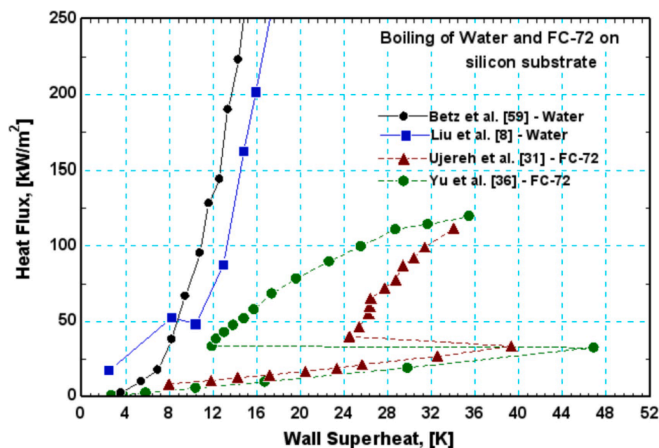

Fig. 3. Comparison between the boiling curve of water and FC-72 on silicon substrates. The boiling curve of water was plotted only for heat flux up to q = 250 kW/m².

low incipience superheat with water compared to FC-72 may be summarized as follows: (i) the silicon surface has cavities of size extremely larger than 0.1 μm, which becomes active with water at low wall superheat but are flooded with FC-72. In fact, the measured superheat with water (8 – 12 K) is corresponding to cavity mouth radius of 2.7 – 4 μm while that of FC-72 is about 0.1 – 0.12 μm. (ii) difference in wettability. Because water is less wetting compared to FC-72, it can trap larger amount of gas, which is obvious from the absence of temperature excursion at incipience. Additionally, as previously discussed in Part I [1], the incipient superheat decreases with the increase of contact angle. Because FC-72 may flood the cavities due to its high wettability, boiling incipience is delayed compared to water. The observed temperature excursion indicates that cavities trap minor amounts of gas with FC-72. (iii) Another possible reason could be the difference in the content of dissolved gases that remained after the degassing process. Degassing was usually conducted by boiling the liquid vigorously for a period of time and releasing the collected gases from a vent in the condenser without any verification to the content of dissolved gases. Variations in the content of dissolved gases may result in variations in the incipience superheat from day to day in the same experiment.

(ii) The slope of the boiling curve is significantly large in the case of water compared to FC-72. This may contradict the analysis conducted in Fig. 23 in Part I [1], which demonstrates that the bubble generation frequency at the same heat flux for FC-72 is much higher than that of water. One might expect that the heat transfer rate of FC-72 and thus the slope of the boiling curve should be larger compared to water due to the larger bubble frequency. It is worth mentioning that frequency is not the only parameter that influence the heat transfer rate. In order to help assess which parameter is important, the latent heat transfer rate per single nucleation site was expressed as: $Q_{site} = \rho_v (\pi D^3/6) f h_{fg}$, where ρ_v is the vapour density, D is the bubble departure diameter, f is the bubble departure frequency and h_{fg} is the latent heat. The vapour density and bubble departure frequency of FC-72 are larger than those of water but the departure diameter and latent heat of water are much larger. Note that the heat transfer rate per site is proportional to D^3. Calculating the latent heat transfer rate per nucleation site at heat flux value 100 kW/m² and 300 kW/m² indicates that q_{site} for water is 30 and 16 times larger than that of FC-72. This may explain, in part, the larger slope of the boiling curve in the case of water. It is interesting to note that if we assume a substrate with size 10 × 10 mm (commonly used in literature) and calculate the heat transfer rate at applied heat flux values 100 and 300 kW/m², the heating power will be 10 and 30 W, respectively. Assuming that, the heat transfer rate due to evaporation accounts for 50 % of the total heat transfer rate, the number of active nucleation sites for water will be about 4 sites at heat flux 100 kW/m² while for FC-72 the calculated number of active nucleation sites will be about 108 sites for the same heat flux. Note that this heat flux value is very low for water while it is near the CHF for FC-72. At a low heat flux value (50 kW/m²) for FC-72, the calculated number of active nucleation site is about 88 sites. In other words, for FC-72, 20 nucleation sites were activated when the heat flux increased from 50 to 100 kW/m². On the contrary, increasing the heat flux to 800 kW/m² for water gave the same number of nucleation sites (4 sites). It is worth mentioning that water requires cavities with large mouth diameter compared to FC-72, which may exist only in small numbers in silicon substrates. This analysis may explain the shape of the boiling curve in Fig. 3. For the highly wetting liquid FC-72, nucleation occurs from sites of about 200 nm and higher, which may exist on the surface in large numbers. This large number of bubbles activated in case of FC-72 may coalesce horizontally and

prevent the liquid supply to cool the surface and thus trigger the CHF. In case of water, it requires cavities of micrometer size, which are expected to be only in small numbers on silicon surfaces. Thus, with few nucleation sites the chance of lateral coalescence is weak which may cause a delay to CHF. This means that the dominant mechanism of CHF depends on the number of active nucleation sites per unit area. Note that this analysis and conclusion is applicable for small size surfaces (10 × 10 mm or so, which is common in literature). Few bubbles could exist and cover the surface at incipience in the case of water due to the larger bubble departure diameter, which may suppress nucleation from other nucleation sites, see Section 2.2 (iii).

2.2. Rough surfaces

It is important to shed some light on the performance of roughened surfaces, which may be considered as a reference for the complex enhancement methods. Table 2 summarizes the heat transfer performance of roughened surfaces for water and dielectric fluids. The table includes the CHF value and the enhancement factors. The following points can be concluded from this table:

(i) Saturated boiling of water on copper surfaces roughened by sandpaper can achieve CHF values up to 1.7 MW/m^2, for Ra = 4.03 μm, at wall superheat 12 (90 % enhancement in CHF and 175 % enhancement in the average HTC). This can be considered as a reference case for the complex enhancement techniques.

(ii) There is agreement on that, the HTC of water on hydrophobic copper surfaces is larger than that of hydrophilic surfaces at very low heat fluxes, e.g. up to 0.06 MW/m^2 [48] and up to 0.33 MW/m^2 [50]. Compared to a reference hydrophilic surface, the HTC was enhanced by 74 % in ref. [50] and 25 % in ref. [48].

(iii) There is contradiction in the effect of surface roughness on the heat transfer performance of water on hydrophobic copper surfaces. Kim et al. [48] reported that the CHF and HTC decrease as roughness increases, while Fan et al. [51] reported an opposite effect. It is worth mentioning that the surface was roughened using sandpaper in these two studies. In the study by Kim et al., the highest CHF was 0.674 MW/m^2 at 13 K superheat for the surface with the lowest roughness and contact angle (0.042 μm and 116^0). On the contrary, the highest CHF value achieved in the study by Fan et al. was 1.25 MW/m^2 at 11.6 K superheat for the surface with the highest roughness and contact angle (1.2 μm and 136^0). It is worth mentioning that in roughened hydrophobic surfaces, the contact angle increases as roughness increases, which is opposite to the roughened hydrophilic surfaces. The reasons of this contradiction are not understood but this may be due to the following reasons: (1) the first reason may be difference in the size of the test section, which may affect the CHF. Kim et al. used 10 × 10 mm test section while Fan et al. used larger test section (20 × 20 mm). The effect of the size of test section arises from the fact that bubble size on hydrophobic surfaces is very large due to larger surface tension force. For example, if the Fritz [56] bubble departure model is used, see Table A3 in Part I [1], with $\theta = 136^0$, the departure diameter is about 7.3 mm, which is nearly equal to the size of the test section used by Kim et al. (10 × 10 mm). In other words, one bubble can cover the whole hydrophobic surface and block the liquid flow from rewetting the surface and thus the CHF is reduced. (2) the second reason could be the method of changing the surface wettability. Kim et al. coated the roughened surfaces by a 50 nm layer of PTFE to make the surface hydrophobic while Fan et al. did not apply any surface coating. Although the coating thickness is very small, its low thermal conductivity may affect the heat transfer performance.

Table 2
Heat transfer performance of roughened surfaces.

Author	Fluid	Material	Surface preparation	Surface roughness, [μm]	θ, [deg]	CHF, [MW/m^2]	Enhancement factor, [–]		ΔT_{CHF} [K]
							HTC	CHF	
Kruse et al. [29]	Water	SS	Femtosecond laser	Ra = 1.4–7.8	Zero	Best surface: Ra = 7.8 μm			
						1.21	2.26	1.34	18.3
Kruse et al. [46]	Water	SS	Femtosecond laser	Ra = 8.2–11.8	Zero	Best surface: Ra = 9.2 μm			
						1.3	1.38	1.43	29
Kim et al. [26]	Water	Al	Sandpaper (unidirectional) and oxidization	Ra = 0.11–2.93	2.7^0–10.4^0	Best surface: Ra = 2.93 μm			
						2.03	1.75	1.27	25.3
Kim et al. [47]	Water	Cu	Sandpaper (unidirectional)	Ra = 0.041–2.36	54^0–70^0	Best surface: Ra = 2.36 μm			
						1.6	2.68	2.14	18.1
Kim et al. [48]	Water	Cu	Sandpaper (unidirectional) coated with 50 nm PTFE layer	Ra = 0.042–1.54	116^0–133^0	Best surface: Ra = 0.042 μm and $\theta = 116^0$			
						0.674	1.25	0.42	13
Walunj and Sathyabhma [49]	Water	Cu	Sandpaper (unidirectional)	Ra = 0.106–4.03	–	Best surface: Ra = 4.03 μm			
						1.69	2.75	1.9	12
Nirgude and Sahu [50]	Water	Cu	Nanosecond laser (parallel lines)	Ra = 0.171–0.29	103^0–114^0	Best surface: Ra = 0.271 μm and $\theta = 103^0$			
						N/A	1.74	–	–
Kruse et al. [23]	Water	Cu	Femtosecond laser	R$_z$ = 17–69.9	Zero	Best surface: sandpaper with $R_z = 17$ μm			
						1.35	1	0.8	17.4
Fan et al. [51]	Water	Cu	Sandpaper (unidirectional) and femtosecond laser (parallel lines)	Sa = 0.045–1.22 (sandpaper), Sa = 0.15–0.38 (laser)	95^0–153^0	Best surface: sandpaper with Sa = 1.2 μm			
						1.25	1.74	1.4	11.6
Mani et al. [52]	Water	Cu	Picosecond laser grooves, width 100 μm, depth (30, 70, 100 μm)	Not measured	Not measured	Best surface: groove depth 100 μm			
						2.26	2.83	2.04	23.2
Jones et al. [53]	FC-77	Al	Electrical Discharge Machine (EDM)	Ra = 0.027–10	Not measured	Best surface: Ra = 10 μm			
						0.19	3.86	1.39	15.1
Fariñas Alvariño et al. [54]	HFE-7100	Brass	Sandpaper	Sa = 0.023–1.878 (sandpaper), S$_q$ = 0.031–2.42	0^0–5.1^0	Best surface: Sa = 0.884 μm, $S^q = 1.16$ μm			
						0.3	2.15	1.5	34.6
Kim et al. [41]	FC-72	Al	Mechanical (unidirectional) and sandpaper (random)	R$_q$ = 0.09–0.86 (sandpaper), R$_q$ = 0.43 (mechanical)	12.6^0–15.9^0	Best surface: sandpaper with $R_q = 0.37$ μm			
						0.22	2.15	1.38	21.6
El-Genk and Pourghasmi [55]	HFE-7000	Cu	Emery paper	R$_q$ = 0.039–0.58	–	Best surface: Ra = 0.58 μm			
						0.295	2.52	1.41	15.2

(3) The third reason could be large uncertainty in the measurement of contact angle. In the study by Kim et al., the contact angle of the plain hydrophilic surface was 65^0 while it was about 95^0 in the study by Fan et al., which is a big difference for the same fluid-surface material. (4) The fourth reason could be uncertainty in the calculation of the applied heat flux which affects the slope of the boiling curve. In the study by Kim et al., the test section was $10 \times 10 \times 3$ mm and was heated by a thin resistance heater attached to the back side, i.e. heat flux was calculated from the power divided by area. Additionally, they did not show any experimental validation. In the study by Fan et al., the test section was a large copper block heated by impeded cartridge heaters and the heat flux was calculated from the measured temperature gradient (Fourier heat conduction equation). Their measurements were validated with the heat transfer model by Rohsenow [57].

(iv) Using laser processing in surface roughening may not lead to reproducible results and some studies reported performance degradation. In fact, the surface microstructure created by laser processing depends on the type and properties of the laser beam, which still need optimization. For example, Fan et al. [51] compared between surfaces roughened by sandpaper and surfaces roughened by femtosecond laser processing. It was found that the enhancements in HTC and CHF was insignificant in the case of laser processed surfaces compared to the plain reference surface. Kruse et al. [23,46] tested saturated boiling of water on stainless steel and copper surfaces enhanced with femtosecond laser, see Table 2 for surface roughness and contact angle. All examined stainless steel surfaces performed poorly compared to the plain reference surface except only one surface with Ra = 9.2 μm, which achieved CHF value of 1.3 MW/m^2 (at 29 K superheat), 38 % enhancement in the HTC and 43% enhancement in CHF. These values are lower than those obtained by surfaces roughened by sandpaper. For all examined copper surfaces, no enhancement in HTC was recorded and the CHF decreased by about 20 %. This performance deterioration was attributed to the formation of oxide layer during the laser processing.

(v) For dielectric liquids, the CHF ranged from 0.2 to 0.3 MW/m^2 at superheat 15–36 K with 40–50% enhancement in the CHF and 115 – 286 % enhancements in HTC. These values may be considered as a benchmark for the complex enhancement techniques discussed in the next sections.

(vi) Most of researchers attributed the enhancement in CHF on the rough surface to enhancements in capillary wicking. For example, Kim et al. [41] tested saturated boiling of FC-72 on aluminum surfaces roughened by sandpaper. The capillary wicking was estimated by measuring the dynamic spreading of liquid droplet on each surface, i.e. the speed and wetting distance of the liquid front was measured using a high-speed camera. It was found that the wetting distance increases with increasing surface roughness (rough surfaces absorb more liquid). However, the CHF did not follow the same trend, i.e. did not increase monotonically with roughness and wetting distance. The highest CHF value was 0.22 MW/m^2 at Ra = 0.37 μm (highest roughness in their study was 0.86 μm).

2.3. Enhanced surfaces

2.3.1. Water on silicon substrates

Table 3 summarizes some experimental studies for saturated boiling of water on enhanced silicon substrates including the CHF value and the enhancement factors. The results of the best performing surface in each study are plotted in Fig. 4 to get an idea about the slope of the boiling curve rather than looking at the CHF value only. Also, Fig. 4 includes pictures for the test surface to understand the microstructure tested in each study. The results of these studies are discussed in the following points:

(i) Wettability has a significant effect on the CHF value. Mohammadi et al. [58] studied the effect of wettability on smooth polished silicon substrates (Ra = 0.35 nm) and changed the wettability in the range 8^0–90^0 by uniform nano-coating. In this wettability range, all boiling curves were merged into one single curve except near the CHF, which was found to decrease significantly with the decrease in wettability. It decreased from 1.25 MW/m^2 to 0.35 MW/m^2 when the contact angle increased from 8^0 to 90^0. This low CHF value (0.35 MW/m^2) agrees with Betz et al. [59] who

Table 3
Heat transfer performance of the best performing surface for saturated boiling of water on silicon substrates.

| Author	Surface microstructure	θ, [deg]	Reference surface	CHF, [MW/m^2]	Enhancement Factors, [-]		ΔT_{CHF} [K]
					HTC	CHF	
Mohammadi et al. [58]	Uniform nano-coating (Ra = 0.35 nm) – effect of wettability	8–90	$\theta = 90^0$	titanium nitride, $\theta = 8^0$ 1.25	2.3	3.6	44.6
Betz et al. [59]	Uniform and non-uniform nano-coating (Ra = 5 nm) – effect of mixed wettability	7–165	Plain surface (SiO$_2$, $\theta = 7^0$)	superbiphilic 1.3	4.6	1.26	8.5
Lim and Bang [12]	Uniform and non-uniform nano-coating – effect of mixed wettability (pattern size 2×2 and 3×3 mm and pitch 4, 5, 6, 8 mm)	42–151	Plain surface (SiO$_2$, $\theta = 41.8^0$)	biphilic surface pattern (2×2 mm) and pitch 4 mm 0.92	1.5	1.15	30.9
Rahman and McCarthy [60]	Uniform coating (Ra = 1–1.5 μm) versus non-uniform coating – effect of mixed wettability	Not reported	Plain surface (other studies)	Superbiphilic surface 1.5	5.4	1.5	10
Liu et al. [8]	Micro-pin-fins ($10 \times 10 \times 50$ μm, pitch 10 μm) at selected areas with uniform and non-uniform coating.	35–100	Plain surface	uniform coating with hydrophilic coating) 2.32	2.1	2.35	28
Liu et al. [9]	square cavities ($210 \times 210 \times 30$ μm) with and without micro-pin-fins etched inside each cavity ($10 \times 10 \times 30$ μm, pitch 10, 20, 30 μm). Only, cavities are coated with hydrophobic coating	144	Plain surface	the surface with fins inside the cavity with fin pitch 10 μm 0.8	1.56	1.15	22.8
Kwak et al. [11]	Parallel rectangular microchannels of width 30 μm and depth 10, 20, 50, 100 μm	60.2	Plain surface	The surface with the deeper channel (100 μm) 2.5	1.9	1.68	41
Yao et al. [10]	Microchannels of width 100–300 μm and depth 150 μm with and without silicon nanowires etched on the channels walls	0–150	Plain surface	the channels with etched nanowires, width 0.1 mm 1.9	3.7	2.7	28
Kim et al. [7]	Surface coated with hexagonal boron nitride (h-BN) of thickness 8–27 μm and Ra value 10.9–15.1 μm	29.6–65.7	Plain surface	the surface with the smallest coating thickness 8 μm and $\theta = 45.2^0$ 1.4	2.3	1.4	20.3
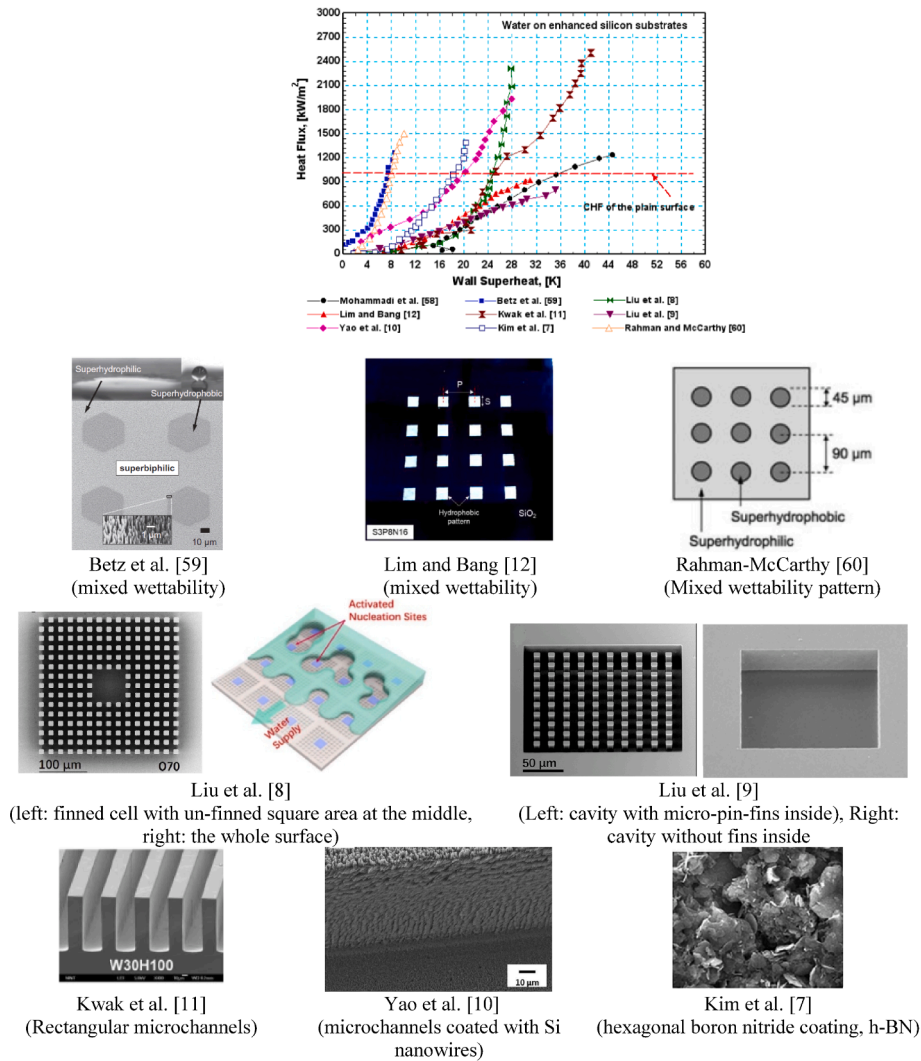
Fig. 4. Saturated boiling of water on enhanced silicon substrates.

reported 0.3 MW/m² and Lim and Bang [12] who reported 0.41 MW/m² for hydrophobic surfaces.

(ii) Some researchers [12,59,60] adopted the hypothesis that boiling heat transfer can be enhanced by mixed wettability rather than uniform wettability. This was conducted by patching a pattern of hydrophobic or superhydrophobic coating on a hydrophilic or superhydrophilic. The surface was called "biphilic" when a hydrophobic pattern is patched on a hydrophilic surface and is called "superbiphilic" when a superhydrophobic pattern is patched on a superhydrophilic surface. Betz et al. [59] tested biphilic and superbiphilic surfaces with hydrophobic and superhydrophobic spots of hexagonal shape (hexagon circle diameter 40 μm and pitch 100 μm). They didn't specify the roughness of the nanostructure of the hydrophilic/superhydrophilic surface but the roughness of the hydrophobic/superhydrophobic spots was <5 nm and its thickness was 100 nm. Lim and Bang [12] designed and tested biphilic surfaces with superhydrophobic spots of square size. They studied the effect of spot size (2 × 2 mm, 3 × 3 mm) and pitch 4–8 mm. They didn't specify the roughness of the surface but the thickness of the superhydrophobic spots was 17 μm. Rahman and McCarthy [60] tested a rough superbiphilic surface (Ra = 1–1.5 μm) with circular spots of superhydrophobic coating (spot diameter 45 μm and pitch 90 μm). The principle idea in these studies was to increase the number of active nucleation sites by reducing the wall superheat

at the hydrophobic spots, restrict the bubble contact area to the area of the hydrophobic spots, regulate the liquid supply to the surface and segregate the vapour and liquid pathways. Thus, lateral bubble coalescence and the size of the dry patches underneath the bubble can be controlled through optimizing the size and pitch of the hydrophobic spots. Rahman and McCarthy didn't test a reference surface. For the sake of comparison, the data of Betz et al. for the reference surface were used. Table 3 and Fig. 4 demonstrates that the boiling curve and enhancement factors given by Betz et al. [59] and Rahman and McCarty [60] are better than those given by Lim and Bang [12], although they adopted the same enhancement mechanism. In these three studies, the CHF was enhanced by 15–50 % while the HTC by 50–440 %. The lowest enhancement was for the surface studied by Lim and Bang [12]. It may be concluded that biphilic surfaces can enhance CHF up to 50 % and HTC up to 440 %. It is worth noting that the coating material and thickness might affect the performance of the boiling surface. For example, Kim et al. [7] coated the surface with hexagonal boron nitride (h-BN) with thickness in the range 8–27 μm and Ra = 10.9–15.1 μm. It was found that the boiling curve shifts to the right as the coating thickness increases, i.e. deterioration of the heat transfer performance. This deterioration was attributed to reduction in the effective thermal conductivity of the coating material due to the voids inside the coating. The coating with the smallest thickness

(8 μm), achieved 130 % enhancement in HTC and 40 % enhancement in CHF with CHF value of 1.4 MW/m². On the contrary, the largest coating thickness achieved CHF value of 1.66 MW/m² (67 % enhancement). However, the wall superheat was extremely high, e.g. 59.3 K. Due to the fact that coating also changes the microstructure, it is difficult to segregate the effect of wettability, i.e. the enhancements may be due to the coating microstructure rather than wettability.

(iii) Some researchers fabricated surfaces with micro pin-fins and studied the effect of biphilic wettability. Liu et al. [8] designed surfaces with micro-pin fins configuration as depicted in the picture in Fig. 4. Fins were etched on square cells on the surface with blank area (un-finned) at the middle of each cell (size of the un-finned area is 70 × 70 μm or 110 × 110 μm). They called the blank area at the middle of each cell "cavity". All cells were spaced by smooth un-finned strips. The principle idea was to coat the cavity only with a hydrophobic coating to create structured surface with biphilic wettability and they also tested surfaces with uniform wettability. Thus, the proposed enhancement mechanism was to activate boiling at low superheat from the hydrophobic cavities (blank area at each cell), improve the lateral capillary flow through the spacing between the fins, regulate the liquid supply to the surface through the smooth un-finned strips, and segregate the liquid and vapour pathways. It is well-known that there are two principles of wetting namely; Wenzel wetting in which the liquid can flood all surface cavities and Cassie-wetting in which air can be trapped inside the surface cavities during the liquid spreading on the surface [86]. Based on the Cassie-wetting principle, Liu et al. [9] used the same experimental setup as [8] and designed a surface with square holes (cavities) of size 210 × 210 μm and spaced with smooth strips. To make the wettability at the cavities of the Cassie-wetting type, they created micro pin-fins inside each cavity to help gas entrapment, see the sixth picture in Fig. 4. Only, the cavities were coated with hydrophobic coating in a similar manner as [8]. From the enhancement factors in Table 3, it can be concluded that the surfaces with micro-pin-fins tested by [8] perform better than those with micro holes (square cavities) tested by [9]. Also, Fig. 4 indicates that the slope of the boiling curve in ref. [9] was much lower than that by ref. [8] where the slope changed to nearly vertical after a certain heat flux value (about 0.5 MW/m²). In the study by Liu et al. [8], the surface with uniform hydrophilic coating (coating the whole surface) performed better than the surface with mixed wettability (biphilic case). The enhancement factors of HTC and CHF were 2.1 and 2.35, respectively with CHF value of 2.3 MW/m² at 28 K superheat. This result contradicts the principle idea based on which the surface was designed, i.e. hydrophobic nucleation sites. The deterioration of the CHF of the biphilic surface was attributed to the large number of active nucleation sites induced by the hydrophobic nucleation sites which results in lateral bubble coalescence and blockage of the liquid supply pathways. The surface tested by Liu et al. [9] with micro-pin fins inside each cavity exhibited slightly better performance than the surface with cavities without fins inside. It is worth noting that both surfaces have the same wettability. The best performing surface in their study achieved 15 % enhancements in CHF and 56% enhancements in HTC with CHF value of 0.8 MW/m².

(iv) Some researchers [10,11] suggested heat transfer enhancements by coated parallel rectangular microchannels. Kwak et al [11] tested channels of fixed width 30 μm and depth in the range 10–100 μm, which were fully coated with a hydrophilic coating, while Yao et al. [10] fabricated channels with width 0.1–0.3 mm and fixed depth 0.15 mm with silicon nanowires etched on the channels-walls including the fins top surface. Increasing the channel height was though by [11] to increase the capillary flow

and reduce the dry patches formed at the fin root, i.e. large coalesced bubbles sit on the fin tops rather than the channel bottom. They found that the CHF reached 2.5 MW/m² on the surface with the deep channels (0.1 mm). Regarding the effect of channel width, Yao et al. [10] found that the best performance occurred with channels of smallest width (0.1 mm) and the CHF value was 1.9 MW/m².

(v) There is no agreement on the CHF of the plain silicon surface. Some researchers [7,8] reported about 1 MW/m², some others [9,10] reported value about 0.7 MW/m² and a third value of 1.5 MW/m² was reported by [11].

In conclusion, it was recommended that saturated boiling of water on silicon substrate can be enhanced with (i) mixed wettability pattern, (ii) coated micro-pin-fins at selective areas, (iii) coated parallel channels, (iv) parallel channels with silicon nanowires on the channels walls, (v) plain surface coating. The CHF values ranged from 0.8 to 2.5 MW/m², the enhancement in CHF ranged from 15 to 170 % and the enhancement in HTC ranged from 56 to 440 %. The highest CHF value was 2.5 MW/m² but the wall superheat was 41 K, i.e. not applicable for example for electronics cooling. For high power electronics, the chip temperature should not exceed 125 °C. Thus, the performance should be assessed in the superheat range up to 25 K for these applications to be included in this analysis. Adopting this approach, the best performing surfaces are: (i) the superbiphilic surface by Rahman and McCarthy [60] which achieved 1.5 MW/m² at 10 K superheat, (ii) the parallel microchannels coated with silicon nanowires proposed by Yao et al. [10] which achieved 1.66 MW/m² at 25 K superheat, (iii) surface coated with hexagonal boron nitride suggested by Kim et al. [7] which achieved 1.4 MWm² at 20 K superheat.

2.3.2. Water on copper substrates

Surfaces with finned structure: Table 4 summarizes the CHF and enhancement factors from studies of boiling on finned surfaces. Figs. 5 and 6 depict the boiling curve and the microstructure for fins/channels fabricated using conventional machining and non-conventional techniques (selective laser melting), respectively. The table shows a wide range of fin/channel geometry including porous and non-porous channels/fins. These studies are discussed briefly as follows:

(i) Non-porous fin/channels: A number of researchers [15,61,62–65] tested saturated boiling of water on copper surfaces enhanced by either parallel channels or pin-fins fabricated using CNC or WEDM. As summarized in Table 4, the investigated geometry includes straight parallel channels [61,63], channels with Ω-shape cross section [15], interconnected microchannels with re-entrant type cavities [62], segmented fins [63], square micro-pin fins [64], and inclined interconnected meso-fins [65]. It can be concluded from these studies that the best performing design was the surface with rectangular parallel channels given by Cooke and Kandlikar [61] which achieved CHF value of 2.44 MW/m² at 9 K superheat (98 % enhancement) and 244 % enhancement in HTC. The second-best surface was the segmented fins structure given by Gouda et al. [63] which achieved 2 MW/m² at 11 K superheat (63 % enhancement) and 273 % enhancement in HTC. It is worth noting that these two designs (parallel channels or segmented fins) are simple and easy to manufacture compared to the other complex designs (see the design by Chen et al. [62]). The performance of the other surfaces [15,62–65] is below the performance of the simply roughened surfaces discussed in section 3.

(ii) Porous fins/channels: Some researchers [14,15,24,66,67,68–70] adopted a combination of fins/channels and porous structure to further increase the enhancement in HTC and CHF. The adopted approaches were as follows: parallel channels coated with sintered copper particles [14,66], sintered copper plate on top of the

Table 4
Saturated boiling of water on finned copper surfaces.

Author	Surface microstructure	CHF, [MW/m^2]	Enhancement Factors, [–]		ΔT_{CHF} [K]
			HTC	CHF	
Cooke and Kandlikar [61]	Microchannels of width (197–400 μm), depth (100–445 μm)–effect of channel geometry,	Channel width 0.375 mm, depth 0.4 mm			
		2.44	3.4	1.98	9
Jaikumar and Kandlikar [66]	Microchannels of width 0.762 mm, depth 0.4 mm – effect of sintered copper coating (channels walls only, only the fins, fully coating)	Fully coated surface			
		3.13	8.5	2.4	7.6
Jaikumar and Kandlikar [14]	Microchannels – effect of channel width (0.3–0.762 mm) for depth 0.4 mm and sintered coating (fully, channels only, fins only)	Channel width 0.3 mm, only walls coated			
		4.2	23.3	3.2	2
Zhang et al. [67]	Microchannels of width 0.8 mm, depth 1.5 mm with sintered copper plate on top of the channels (thickness 2, 3, 4 mm)	Sintered plate thickness 4 mm			
		6.5	3.2	4.2	53.5
Chen et al. [62]	Interconnected microchannels (0.8 × 1.6 mm) with re-entrant cavities	Interconnected with re-entrant cavities			
		1.64	3	1.36	21.3
Gouda et al. [63]	Parallel microchannels (0.4 × 0.45 mm) versus segmented channels	Surface with segmented fins			
		2	3.73	1.63	11
Hai et al. [64]	Square pin-fins of height 0.2 mm, pitch 0.1 mm and cross section 0.4 × 0.4 mm, 0.8 × 0.8 mm and 1 × 1 mm	Fin cross section 0.8 × 0.8 mm			
		1.51	2.16	1.7	5
Safari et al. [65]	Inclined interconnected meso-fins, effect of fin size and geometry and inclination angle on the vertical direction.	Fins with inclination angle 45^0 and height 1.2 mm			
		1.22	3.4	1.4	5.7
Deng et al. [15]	Channels of Ω-shape cross section (total depth 1.1 mm, width 0.4 mm, upper depth 0.3 mm, circular diameter 0.8 mm) versus the same geometry but cut in a sintered copper plate (solid versus porous channels)	The porous channels			
		1.17	0.84	1.16	61
Pi et al. [68]	The same geometry as Deng et al. [78] but fabricated by selective laser melting (SLM)	SLM Ω-shape channels			
		1.67	1.24	1.69	35.8
Cho et al. [69]	Micro-patterned surface consisting of square micro-pin fins 0.1 × 0.1 mm, pitch 50 μm and height 0.1–0.38 mm fabricated by powder injection molding	Pin-fins with the shortest height			
		1.42	1.13	1.3	26
Wu et al. [24]	Porous channels of width 0.3 mm and depth 0.5, 1 mm fabricated by selective laser melting. The fins were hollow with hexagonal holes on the top and side walls to create porous wall.	The surface with fins height 1 mm			
		4.55	1.96	2.7	27.8
Elkholy and Kempers [70]	Low conductivity porous polymer fixture fabricated by additive manufacturing. The texture consisted of square cavities and was attached to the copper surface by plastic screw. Effect of cavity size and height.	Cavity size 4.3 × 4.3 mm and height 2 mm			
		1.71	1.32	1.15	24.4

channels [67], channels of Ω-shape cross section cut in sintered copper plate [15], channels of Ω-shape cross section made by selective laser melting (produces porous structure) [68], pattern of square micro-pin-fins using powder injection molding (create porous structure) [69], parallel channels with hollow fins and holes on the top and side walls made by selective laser melting [24], and porous polymer fixture fabricated by additive manufacturing [70]. The highest achieved CHF value was 6.5 MW/m^2 for a microchannel surface (diameter 8 mm) with sintered copper plate on top of the channels given by Zhang et al. [67]. However, the wall superheat at this heat flux value is 53.5 K. Additionally, the HTC enhanced by 220 %. The authors [67] tested another surface but with smaller test section diameter (6 mm) and reported superior enhancement in CHF, which reached 8.06 MW/m^2. However, the wall superheat at this value was 250 K, which is far from being practical. The second highest CHF value was 4.55 MW/m^2 at 27.8 K superheat for a surface consisting of parallel channels with hollow fins and hexagonal holes on the top and side walls designed by Wu et al. [24] and fabricated using selective laser melting. This surface enhanced the HTC by 96 %, i.e. the slope of the boiling curve is low. The third highest CHF was 4.2 MW/m^2 at 9 K superheat for parallel microchannels with sintered copper particles applied to the channels walls only given by Jaikumar and Kandlikar [14]. Also, this surface achieved superior enhancements in HTC, which was up to 2230 %. The surfaces studied by [15,68–70] performed poorly or similarly to the simply roughened surfaces discussed in section 3. Thus, it can be concluded that the best surface in terms of CHF and HTC was the one given by Jaikumar and Kandlikar [14].

(iii) The review of the above studies indicated that three studies reported very high CHF values compared to the other studies. The evaluation of the enhanced surfaces in this section will be based on superheat up to 25 K so that results can also be applicable for electronics cooling. The microchannels structure (width 0.3 mm, depth 0.4 mm) with only coating the channels walls with sintered copper particles suggested by Jaikumar and Kandlikar [14] exhibited the best heat transfer performance among all studies with CHF value of 4.2 MW/m^2 at 2 K superheat, i.e. more than 300 % enhancements in CHF and 2200 % enhancement in HTC. The second highest CHF value was reported by Zhang et al. [67] which was 4.1 MW/m^2 at 25 K superheat for parallel channels with sintered copper plate on top of the channels. The CHF was similar to Jaikumar and Kandlikar but the superheat was significantly larger. The third study was by Wu et al. [24] for parallel channels with hexagonal holes along the fins and the top and side walls. It achieved 4.1 MW/m^2 at 25.8 K superheat which is nearly similar to Zhang et al. [67]. These enhancements may be due to the large surface area of the microchannels.

Surface Coating: Figs. 7 and 8 compare the boiling curve for saturated boiling of water on coated copper surfaces along with the SEM images in each study. These studies are summarized in Table 5 along with the CHF
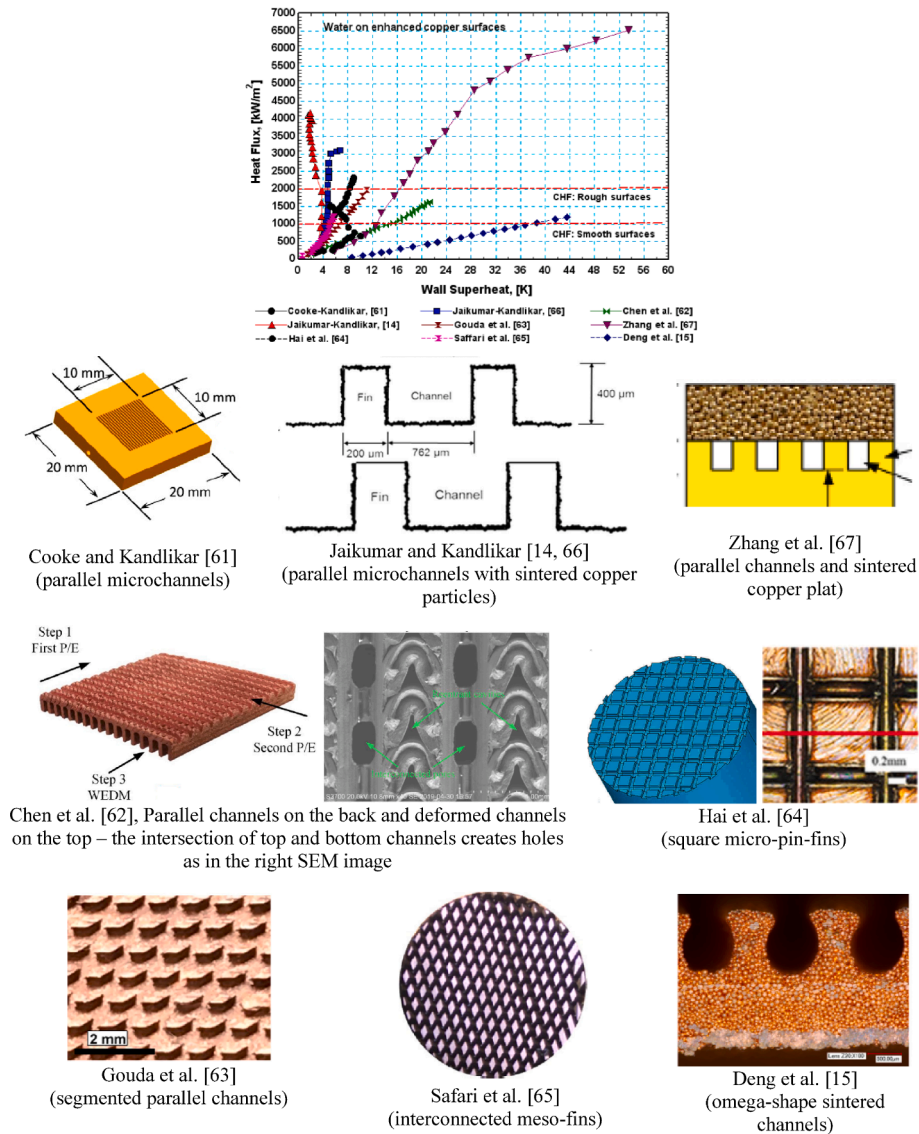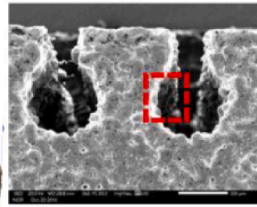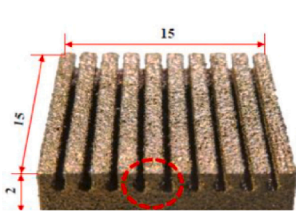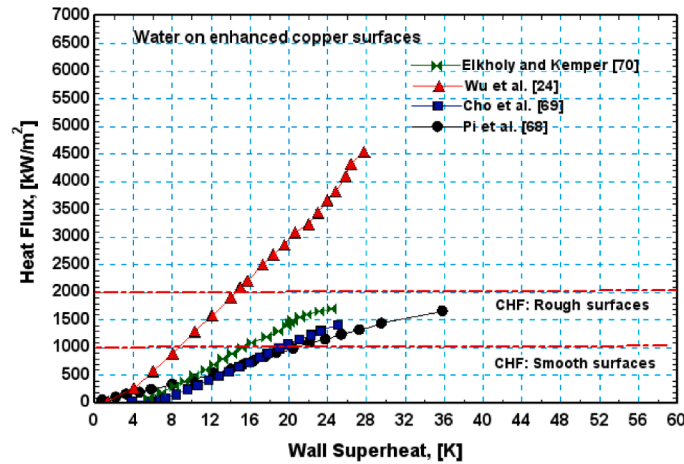
Fig. 5. Saturated boiling of water on copper surfaces with fins structures (with or without porous layer).

value and the enhancement factors for the best performing surface. The following points can be concluded from these studies:

(i) Different techniques were tested by a number of researchers [5,16,25,71], which include the self-assembly method in which the coating material is dispersed in a liquid to create a nanofluid then the coating is deposited to the surface by boiling the prepared nano-fluid. Some other researchers coated the surface by sintering copper particles [13], cold sprayed copper-diamond composite particles [22], using copper particles in a binding paste [72] and electron-beam vapour deposition [17] in which the coating material is vaporized using the electron-beam. Other techniques are the dip-coating or sol–gel [73,74], in which the substrate is immersed in a solution that contains the coating material, and supersonic spraying technique [75]. Another group of researchers [18–21,76,77] deposited the coating using electrochemical deposition and their results for the best performing surface is plotted in Fig. 8.

(ii) Some researchers tested surfaces with modulated porous structure (porous pillars/channels) and compared with surfaces of flat porous layer. The modulated structure was assumed to help regulate the liquid supply to the surface and segregate the liquid

and vapour pathways which increases the CHF. Khan et al. [5] tested a surface coated with CuO nanoparticles (25–50 nm), a surface coated with modulated (v-shaped channels) copper particles (0.2 mm) and a surface with hybrid coating (modulated sintered particles coated with CuO nanoparticles). It was found that, compared to the plain surface, the nanocoated surface achieved 81.6 % enhancement in CHF and 130 % enhancement in HTC with CHF value of 1.5 MW/m^2 at 40 K superheat while the surface with modulated porous particles achieved 50.6 % enhancement in CHF and 45 % in HTC with CHF value of 1.2 MW/m^2 at 39 K. It means that the modulated porous structure did not add significant enhancements although their principle idea was to regulate the vapour and liquid pathways and thus increase the CHF. The performance gets worse with the hybrid coating, where the boiling curve was shifted to the right of the plain surface. Rioux et al. [13] tested a combination of nano and micro structure. The nanostructure was created by acid etching and the microstructure was created by sintered copper particles. They tested five scenarios: (i) etched surface, (ii) sintered copper layer (1 mm thick, particle size 0.5 mm), (iii) modulated sintered copper particles on top of a 1 mm thick sintered layer (cylindrical pillars 4 mm diameter and 3 mm height), (iv) acid etched surface
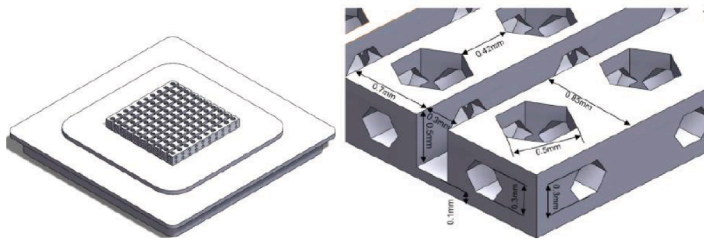
Pi et al. [68]
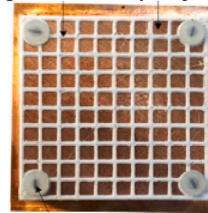(Channels of omega-shape cross section by SLM)
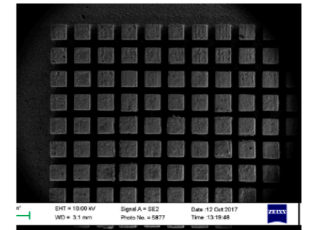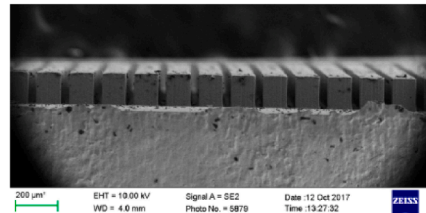
Cho et al. [69]
(Square fins by injection powder molding)

Wu et al. [24]

Elkholy and Kemper [70]

Fig. 6. Saturated boiling of water on copper surfaces with fin structure created by non-machining techniques.

coated with sintered layer of copper particles, and (v) acid etched surface coated with modulated sintered particles. It was found that the surface with nanostructure (etched surface) alone achieved 28 % enhancement in the CHF compared to the plain surface, while the surface with sintered layer enhanced the CHF by 100 %. The surface with modulated structure enhanced the CHF by 170 % compared to the plain surface. It can be concluded that the best performing surface is the one with hybrid structure (etched nanostructure and modulated sintered particles) with enhancement factors in CHF and HTC are 3.1 and 5.9, respectively. This structure achieved a CHF value of 3.78 MW/m^2 at 21.3 K superheat.

(iii) Some researchers such as Souza et al. [16] reported that the coating can result in deterioration of the heat transfer performance compared to the plain surface. They coated the surface with aluminum oxide and this deterioration was attributed to the additional thermal resistance of the coating and filling of the cavities with the nanoparticles which reduces the original cavity size. Some other researchers, Mao et al. [25], found that the boiling curve of the coated surface was the same as the uncoated surface except that the CHF of the coated surface was higher, i.e. the boiling curves are coincident with the coated surface extends to higher CHF value. They coated the surface with graphene oxide nanoparticles (0.8 μm thickness). The enhancement factors in

CHF and HTC were 1.77 and 1.3 respectively with CHF value of 2.14 MW/m^2 at 24 K superheat. Note that the area under the curve (HTC versus heat flux) that is used to calculate the heat-flux averaged HTC is larger in case of the coated surface compared to the plain surface.

(iv) Few researchers tested the surface aging, which may affect the performance of the enhanced surfaces. Mo et al. [77] tested surfaces with a porous honeycomb structure created by electrochemical deposition (pore size 60–120 μm and thickness 120–180 μm). They conducted the test several times and reported that the performance gets better with time after the surface oxidized compared to the first run. The enhancement factors of this oxidized surface were 1.15 for the CHF and 4.9 for the HTC.

(v) The review of the studies summarized in Table 4 indicated that a wide range of coating material was tested: sintered copper particles, graphene, graphene oxide, aluminum oxide, aluminum silver oxide, copper oxide, silver nanowires, composite coating of copper and aluminum oxide, copper-titanium oxide composite coating and copper nanowires. The highest CHF values were 3.78 MW/m^2 at 21.3 K superheat by Rioux et al. [13] for acid etched surface with modulated sintered copper particles and 3.1 MW/m^2 at 25 K superheat by Mori et al. [71] for a surface coated with TiO$_2$ and commercial honeycomb porous plate. At lower degree of superheat, Rishi et al. [18] reported 2.9 MW/m^2 at 14 K for
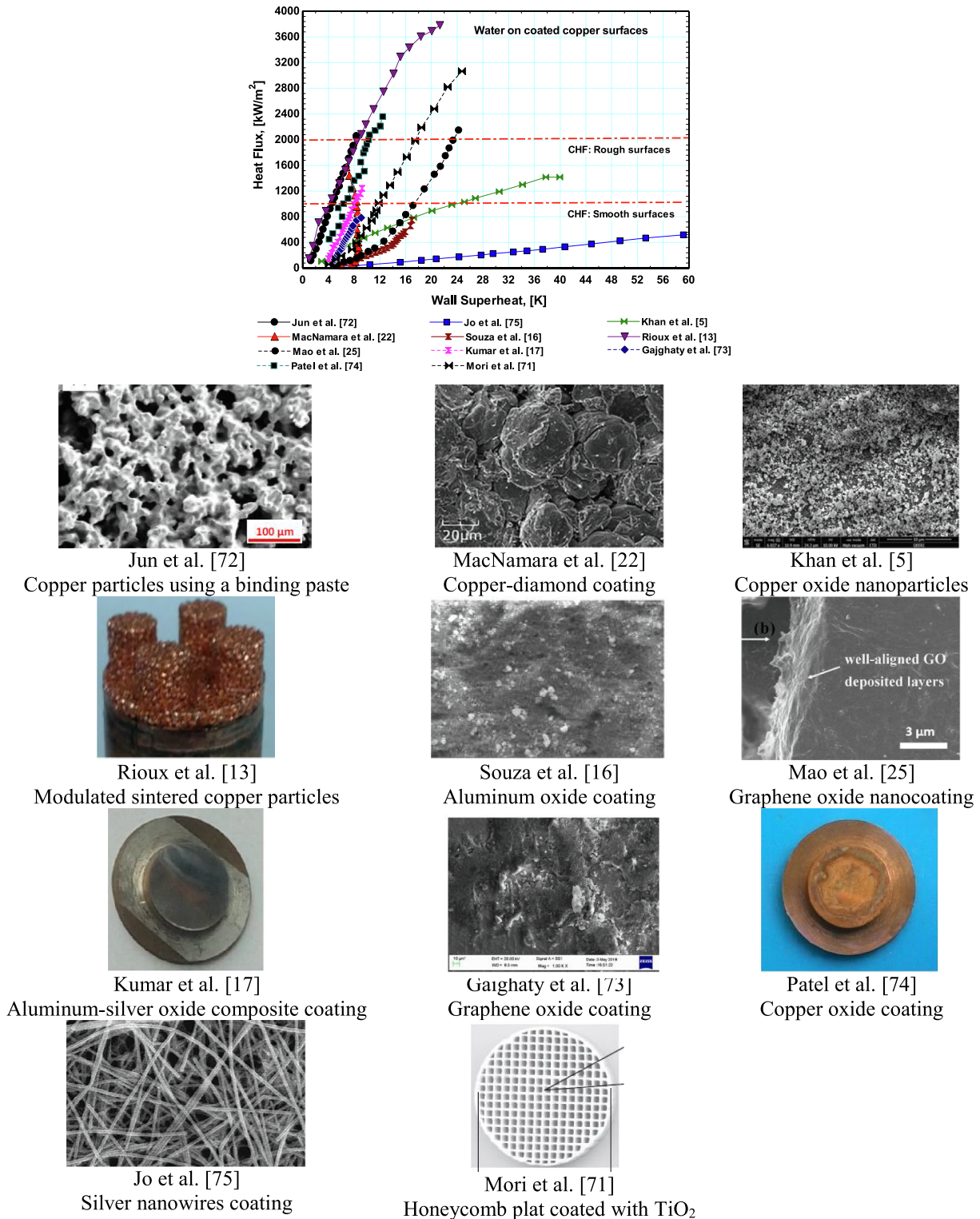
Fig. 7. Saturate boiling of water on coated copper surfaces.

graphene nanoplatelets-copper coating, Chen and Li [20] gave 2.46 MW/m^2 at 17 K superheat for a grooved surface with Cu nanowires. Also, the surface coated with copper oxide by Patel et al. [74] achieved 2.4 MW/m^2 at 12 K superheat.

2.3.3. FC-72 on silicon substrates

Fig. 9 depicts the boiling curve for saturated and subcooled boiling of FC-72 on enhanced silicon substrates along with pictures for the tested microstructure. The description of these studies is summarized in Table 6. The concluding remarks from these studies are as follows:

(i) Some researchers enhanced the surface using random micro-structure of either carbon nanotubes (CNTs) [31,78] or femto-second laser processing [32,79]. Ujereh et al. [31] coated the surface with CNTs of diameter 50 nm and length range 20–30 μm and tested uniform coating versus non-uniform coating (coating
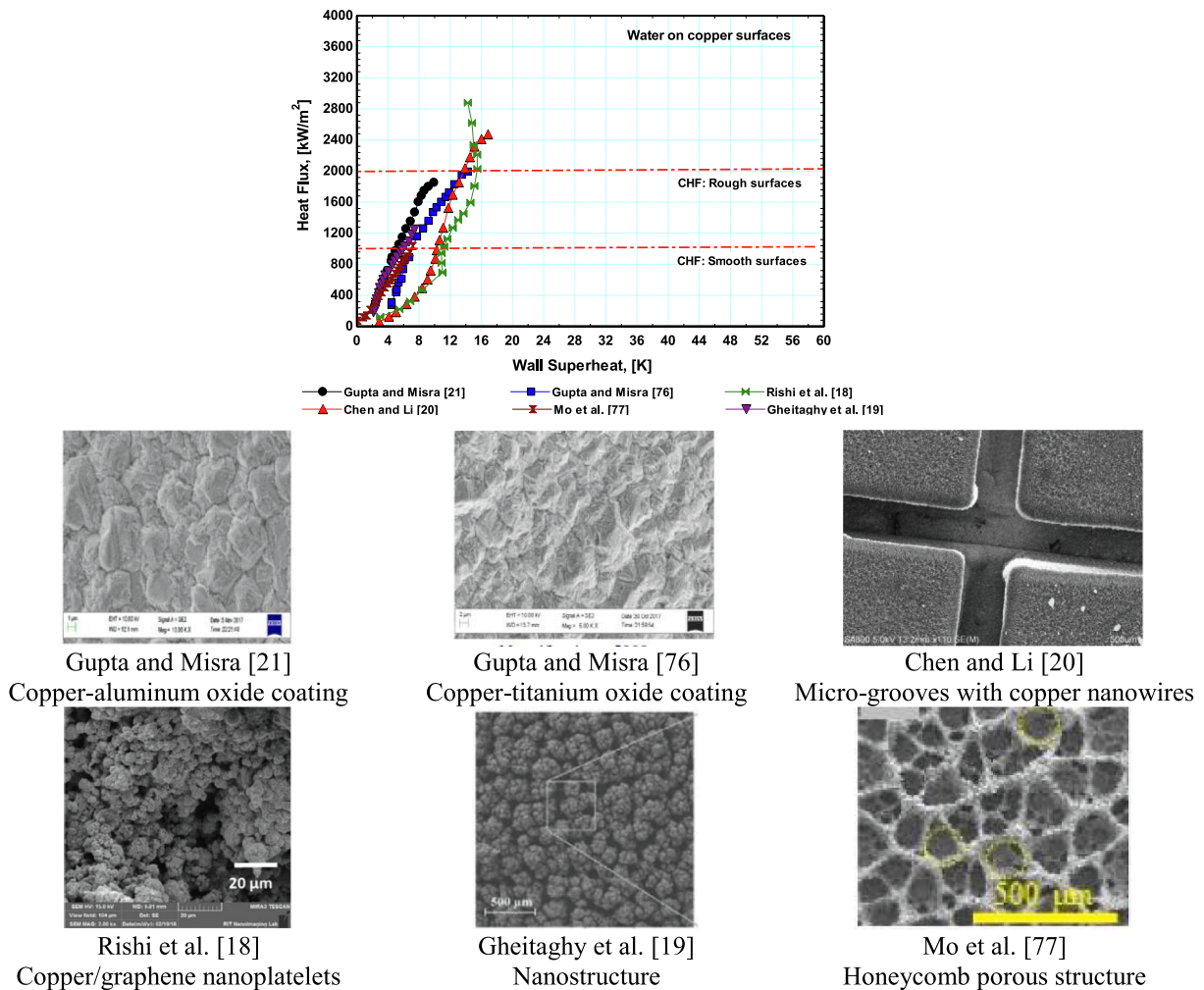
Fig. 8. Saturated boiling of water on copper surfaces enhanced by electrochemical deposition.

applied only at small squares or circles). It was found that the uniformly coated surface achieved the best performance compared to the non-uniform coated surfaces. The enhancement factors in HTC and CHF of the uniformly coated surface were 1.54 and 4.64, respectively with a CHF value of 0.172 MW/m^2 at 11.8 K. This enhancement was attributed to the increased lateral thermal conductivity induced by the carbon nanotubes, increased surface area, improved capillary flow in the lateral direction and the increased number of nucleation sites. Ahn et al. [78] studied the effect of the CNTs length (9 and 25 μm) in a uniformly coated surface. It was found that the effect of the nanotube's length was insignificant and the CHF value of the coated surface was 53 kW/m^2 at 86 K wall superheat (very high superheat). This gives enhancement factors of 1.4 for both the CHF and the HTC. They attributed the low CHF value and enhancements in HTC, compared to Ujereh et al. [31], to the method of synthesizing the CNTs. This reason may not be appropriate because the CHF value of the uncoated plain surface in their study was also much lower (48 kW/m^2 at 87 K superheat) compared to Ujereh et al. [31] (CHF of plain surface was 111 kW/m^2 at 34 K). Liu et al. [32] enhanced the surface by femtosecond laser processing conducted in the x and y directions and studied the effect of the pitch (30–800 μm) and depth (peak-to-valley 35–101 μm). It was found that the boiling curve of the processed surfaces was nearly vertical up to a heat flux value of about 0.15 MW/m^2 after which the slope of the curve decreased significantly up to the CHF. Among the examined surfaces, the surface with processing pitch 200 μm

and peak-to-valley 101 μm exhibited the best performance. The enhancement factors of this surface were 1.9 and 3.95 for CHF and HTC, respectively with a CHF value of 0.31 MW/m^2 at 38 K superheat. They attributed this enhancement to the increased number of nucleation sites and enhancements in the liquid supply through the smooth unprocessed strips. Liu et al. [79] extended the work reported in [32] to include the effect of subcooling (1–35 K). It was found that the CHF increases with increasing subcooling where the highest value was 0.54 MW/m^2 at 21 K superheat and 35 K subcooling. The enhancement factors at 35 K were 2.1 and 3.1 for CHF and HTC, respectively. Additionally, the effect of subcooling on the boiling curve was insignificant for heat fluxes below the CHF.

(ii) Another group of researchers [33–35,80,81] adopted the premise that heat transfer can be enhanced by improving the capillary flow in the lateral direction and leaving plain areas to help the liquid supply to the surface and segregate the liquid and vapour pathways. Thus, they fabricated micro-pin-fins structure using deep reactive ion etching and tested several configurations, e.g. uniform fins distribution versus non-uniform distribution. Zhou et al. [33] designed five surfaces with aligned square micro-pin-fins, which were distributed in a complex way according to what is called "fractal dimension", see the picture in Fig. 9. The first surface has one finned square area (6.99 × 6.99 mm) at the middle and the second has four finned square areas of size 3.51 × 3.51 mm (one area at each corner). Each finned square area in the second surface was split into four areas progressively with area

Table 5

Saturated boiling of water on coated copper surfaces.

Author	Surface microstructure and preparation	CHF, [MW/m²]	HTC	CHF	ΔT_CHF
Jun et al. [72]	Copper particles (25 μm) mixed with a binding past of thickness 50–280 μm – effect of coating thickness	*Coating thickness 225 μm* 2.1	9.8	2	8
MacNamara et al. [22]	A mixture of diamond and copper of coating thickness 0.4 mm	*Diamond-copper coating* 1.6	2.54	1.34	7
Khan et al. [5]	Surfaces uniformly coated with CuO nanoparticles (25–50 nm), sintered modulated (V-shape) copper particles, hybrid coating (Cu modulated structure and deposited Cu nano-particles)	*Uniformly nano-coated surface* 1.42	2.1	1.75	40
Rioux et al. [13]	Acid etched surface, surface with uniform sintered copper layer (0.5 mm diameter and 1 mm thickness), surface with modulated sintered particles (uniform layer 1 mm thick on top of which there are sintered cylindrical pillars of 4 mm diameter and 3 mm height, hybrid structure (etching and sintering).	*Hybrid structure of acid etching and modulated sintered copper particles* 3.78	5.9	3.1	21.3
Souza et al. [16]	Smooth and rough surfaces coated with aluminium oxide	*Smooth coated surface* 0.74	0.96	0.94	17
Mo et al. [25]	Graphene oxide nanocoating of thickness 0.8 μm	*Graphene oxide nanocoating* 2.14	1.3	1.77	24
Kumar et al. [17]	Surface coated with aluminium-silver oxide of thickness 0.18 and 0.26 μm.	*Surface with coating thickness 0.26 μm* –	1.3	–	–
Gajghate et al. [73]	Surface coated with graphene of thickness 97–400 nm.	*Surface with coating thickness 400 nm* –	1.36	–	–
Patel et al. [74]	Surface coated with copper oxide of thickness 200 and 400 nm	*Surface with coating thickness 400 nm* –	1.9	–	–
Jo et al. [75]	Surface coated with silver nanowires with thickness 35–255 nm	*Surface with coating thickness 144 nm* 0.65	3.4	3.5	76
Mori et al. [71]	Surface coated with titanium oxide nanoparticles and on top of the surface there is a commercial honeycomb plate of pore size 1.4 × 1.4 mm and 1 mm thickness. Test section diameter was 10, 30, 50 mm.	*Coated surface of diameter 10 mm and honeycomb plate* 3.1	1.45	2	24.7
Gupta and Misra [21]	Surface coated with copper–aluminium composite nano-coating with coating thickness 13–45 μm.	*Surface with coating thickness 45 μm* 1.85	4.7	1.7	9.9
Gupta and Misra [76]	Surface coated with copper-titanium oxide composite nano-coating with coating thickness up to62 μm.	*Surface with coating thickness 62 μm* 2	3.3	1.8	14.1
Chen and Li [20]	Surface with micro grooves of width 0.262 mm, depth 0.518 mm and pitch 0.5, 1 and 4 mm (similar to square pin fins) coated with	*Grooves of pitch 0.5 coated with copper nano wires of height 25 μm* 2.64	2.2	2.2	16.8

Table 5 (*continued*)

Author	Surface microstructure and preparation	CHF, [MW/m²]	HTC	CHF	ΔT_CHF
Rishi et al. [18]	copper nanowires of height 5, 15, 25 μm. Surface coated with graphene nanoplatelets-cupper porous coating. The concentration of the graphene nanoplatelets ranged from 0.25 to 2.5%.	*Surface with 2 % graphene concentration* 2.86	2.9	2.3	14.2
Gheitagy et al. [19]	Nanostructure created by electrochemical deposition – effect of electrolyte temperature	*Dendritic structure created at electrolyte temperature 60 °C* 1.25	3.1	1.47	7.4
Mo et al. [77]	Honeycomb porous structure created by electrochemical deposition. Uniform pore size of 60 and 120 μm and a surface with pore size that increases from the centre towards the outer edges of the surface (from 60 to 120 μm).	*Surface with por size gradient* 1.03	4.9	1.15	7.2

size shrinking to 1.77 × 1.77 mm, 0.87 × 0.87 mm, and 0.45 × 0.45 mm in the third, fourth and fifth surface, respectively. They also included in the comparison a surface with uniformly distributed fins. It was found that the boiling curve of the surface with uniformly distributed fins exhibited the best heat transfer performance with nearly vertical slope. This surface enhanced the CHF by 66.9 % in saturated boiling and 121.6 % at 35 K subcooling. The enhancement factors in saturated boiling were 1.67 and 2.8 for CHF and HTC respectively, with CHF value 0.26 MW/m² at 19 K superheat. The enhancement factors in subcooled boiling (35 K) were 2.26 and 4.16 for CHF and HTC respectively, with CHF value of 0.48 MW/m² at 15 K superheat. It can be concluded that the non-uniform pattern distribution did not create additional enhancement compared to the uniformly distributed pattern. It is worth mentioning that they reported that the non-uniform distribution achieved significant enhancement compared to the uniform structure. However, inspecting their results, one can see that the difference in CHF between the uniform and non-uniform distribution was less than 10 % for saturated boiling. Duan et al. [34] tested five surfaces enhanced with aligned cylindrical micro-pin-fins of fixed height 120 μm but different fin diameter. The fins were uniformly distributed in the first three surfaces; fin diameter 25 μm (surface 1), 50 μm (surface 2), and 100 μm (surface 3). In the other two surfaces, the fins were distributed only at rectangular areas (non-uniform distribution) with mixed fin diameter (combination of the 25, 50 and 100 μm diameter). They concluded that surfaces with nonuniform fins distribution of mixed diameters show excellent heat transfer performance compared to the fins with uniform distribution. However, their data indicates that the surface with uniform fin distribution of fin diameter 50 μm exhibited the best heat transfer performance. The boiling curve of this surface was nearly similar to that with non-uniform distribution. The only difference was that the CHF value of the non-uniform distribution was slightly higher (6 % difference). In saturated boiling and the uniformly distributed fins, the enhancement factors in CHF and HTC were 1.74 and 2.46, respectively with CHF value of 0.271 MW/m² at 25.3 K superheat. This CHF value was nearly the same regardless of the fin distribution pattern. In subcooled boiling (25 K), the enhancement factors in CHF and HTC were 2.3 and 5.9 with CHF value of 0.51 MW/m² at 19.9 K superheat. The enhancement in
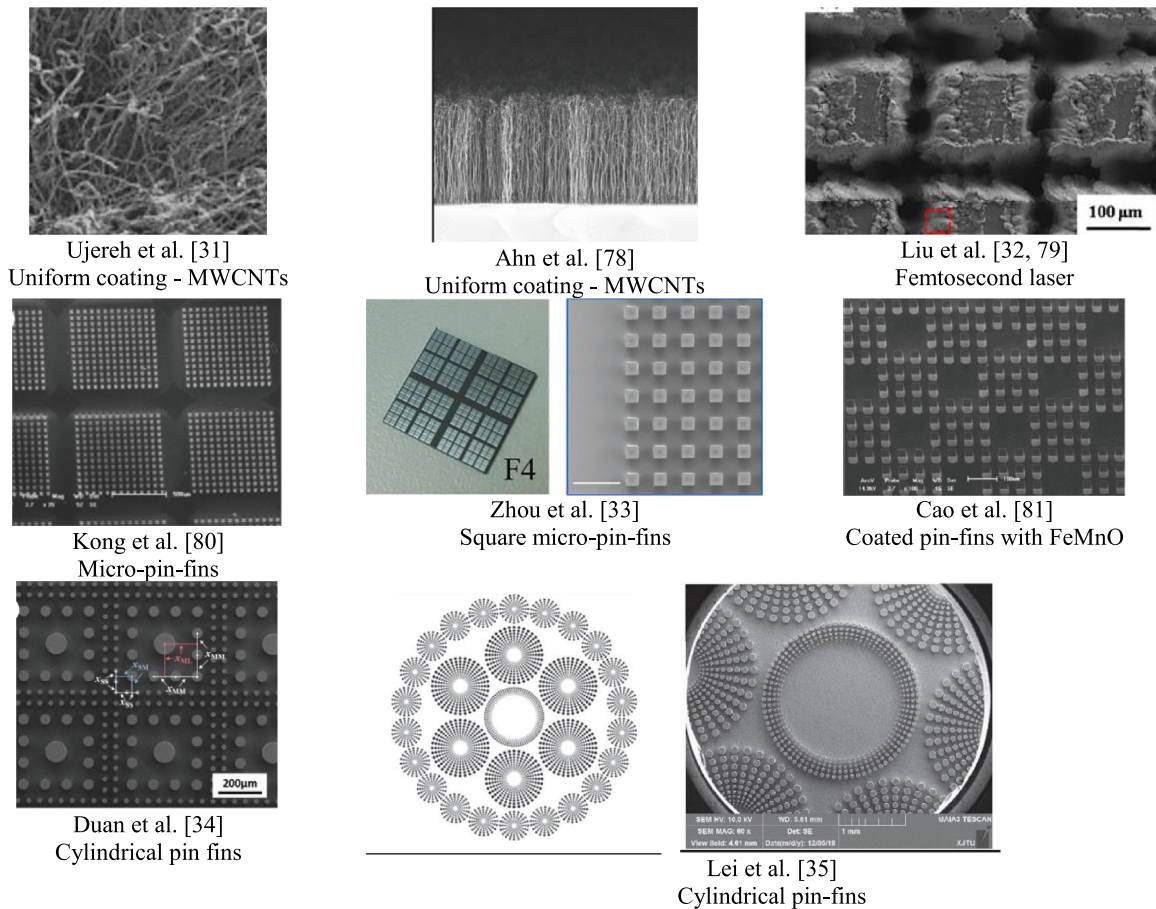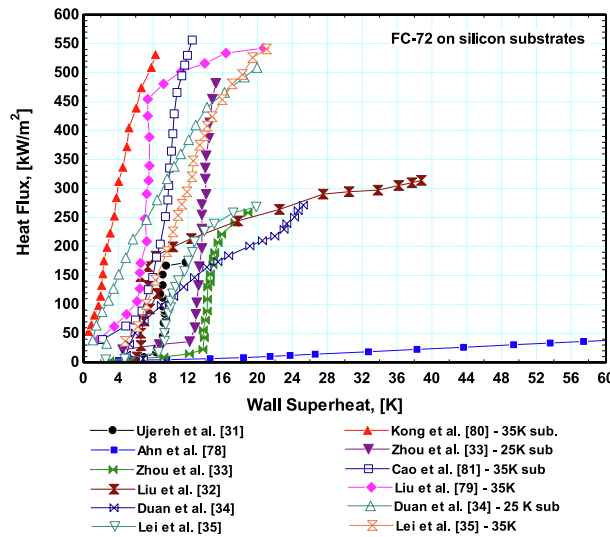
Fig. 9. Saturated and subcooled boiling of FC-72 on enhanced silicon substrates.

saturated boiling was attributed to the enhancement in surface area and increased number of nucleation sites. The reduction in CHF in saturated boiling compared to sub-cooled boiling was attributed to the larger bubble departure size and thus the larger chance of coalescence in saturated boiling. This reduces the liquid supply to replenish the surface. Lei et al. [35] conducted a work similar to Duan et al. [34] using mixed diameters of cylindrical micro-pin-fins but distributed at circular areas. In each circular area, the fins were distributed radially with a blank area at the middle and the fin diameter increased in the radial direction. They varied the number of the finned areas and the size of

the blank circle at the center of each large circle (0.2 to 1.8 mm), see the picture in Fig. 9. It was found that the surface that has a combination of circles with blank diameter ranging from 0.2 to 1.8 mm exhibited the best performance. In saturated boiling, this surface achieved enhancement factors in CHF and HTC of 1.65 and 2.6, respectively with CHF value of 0.26 MW/m^2 and 26.5 K superheat. In subcooled boiling (35 K), the enhancement factors were 2 and 1.6, respectively with CHF value of 0.53 MW/m^2 at 20.8 K superheat. Kong et al. [80] designed surfaces with square micro-pin-fins distributed in parallel strips compared to surfaces with the fins distributed at square areas. It was found that the

Table 6

FC-72 on silicon substrates.

Author	Surface microstructure	CHF, [MW/m^2]	Enhancement Factors, [–]		ΔT_{CHF} [K]
			HTC	CHF	
Ujereh et al. [31]	Multi-walls carbon nanotubes of diameter 50 nm and length 20–30 μm. Fully coating, grid pattern coating of pitch 5 mm, and coating on 2D array of circular areas of diameter 0.25 mm and pitch 1 mm	Fully coated surface, saturated boiling			
		0.17	4.6	1.5	11.8
Ahn et al. [78]	Fully coated surface with multi-walls carbon nanotubes of diameter 8–15 nm and length 9 and 25 μm.	Nanotube length does not have significant effect, saturated boiling			
		0.053	1.4	1.4	86
Liu et al. [32]	Femtosecond laser processing in × and y directions with spacing 30–800 μm between the laser beams and roughness peak to valley 35–101 μm	Laser spacing 200 μm and peak to valley 101 μm			
		0.31	3.95	1.9	38
Liu et al. [79]	The same structure as [95] but at sub-cooling 1–35 K	Sub-cooling 35 K			
		0.54	3.1	2.04	20.7
Kong et al. [80]	Surfaces with micro-pin-fins (30 × 30 × 60 μm and 60 μm pitch) in different configurations at sub-cooling 15–35 K. Surface fully finned, surface with fins distributed at parallel strips (width 0.7 and 1.4 mm) separated by smooth un-finned strips of width 0.3 and 0.5 mm, surface with fins distributed at square areas (0.7 × 0.7 mm and 1.4 × 1.4 mm) separated by smooth strips of width 0.3 and 0.3 mm.	Surface with fins distributed at square areas separated by 0.3 mm at 35 K sub-cooling			
		0.52	3.8	2.3	8.2
Zhou et al. [33]	Surfaces with micro-pin-fins (30 × 30 × 60 μm and 60 μm pitch) distributed at square areas on the surface compared to uniformly distributed fins on the whole surface. They tested wide range of finned area size and the smooth spacing between each finned area. The sub-cooling ranged from 0 to 25 K	Uniformly distributed fins on the whole surface			
		Saturated			
		0.26	2.83	1.7	19
		35 K sub-cooling			
		0.48	4.16	2.26	15
Cao et al. [81]	Surfaces with micro-pin-fins (30 × 30 × 60 μm and 60 μm pitch) uniformly distributed with staggered arrangement and other surfaces with fins aligned and distributed at selective square areas on the surface. The effect of nanocoating (FeMn oxide) was studied and sub-cooling was 15–35 K.	Surface with aligned fins at selective square areas and coated with FeMn oxide at 35 K sub-cooling			
		0.56	2.9	2.2	12.5
Duan et al. [34]	Uniformly distributed cylindrical micro-pin fins of fixed height 120 μm and diameter 25, 50, 100 μm (three surfaces). Two surfaces with fins distributed at selective rectangular areas with mixed fin diameter (fin diameter decreases from	Uniform fin distribution with fin diameter 50 μm			
		Saturated			
		0.271	2.46	1.74	25.3
		25 K sub-cooling			
		0.51	5.9	2.3	19.9

Table 6 (*continued*)

Author	Surface microstructure	CHF, [MW/m^2]	Enhancement Factors, [–]		ΔT_{CHF} [K]
			HTC	CHF	
	the centre of each rectangle towards the sides).				
Lei et al. [35]	Cylindrical micro-pin fins of fixed height 120 μm distributed at selective circular areas on the surface with a blank circular area at the middle (diameter 0.2–1.8 mm). The fin diameter increased in the radial direction (diameter range 25–255 μm). saturated and subcooled boiling up to 35 K.	A surface with combination of circular finned areas at selective locations on the surface			
		Saturated			
		0.26	2.6	1.65	26.5
		35 K sub-cooling			
		0.53	2	1.6	20.8

performance of the surface with finned square areas was slightly better than that of parallel strips. The CHF value of the surface with square finned areas was 0.52 MW/m^2 at 8.2 K superheat and 35 K subcooling (they did not study saturate boiling). This surface achieved enhancement factors in CHF and HTC of 2.3 and 3.8, respectively. Cao et al. [81] studied the effect of coating the fins with FeMn oxide nanoparticles. They tested square micro-pin-fins (with and without coating) in two different configurations: uniform distribution in staggered arrangement and non-uniform distribution (at square areas) in aligned arrangement. It was found that the aligned fins in non-uniform pattern (square areas) with coating the whole surface achieved the best performance. The enhancement factors of this surface were 2.2 and 2.9 for CHF and HTC, respectively. The CHF value was 0.56 MW/m^2 at 12.5 K superheat and 35 K sub-cooling (they did not study saturated boiling).

It can be concluded from the above studies that, even with these complex arrangements of fin structure, the CHF value of FC-72 on silicon substrates is about 0.3 MW/m^2 in saturated boiling and 0.5 MW/m^2 in sub-cooled boiling (35 K). The surfaces enhanced with femtosecond laser processing, which may be a fast process compared to the complexity of deep reactive ion etching, gave similar enhancements. In saturated boiling, the enhancement in the HTC was in the range of 160–360 % and the CHF in the range of 50–90 %. In sub-cooled boiling the HTC was enhanced by 100–490 % and the CHF by 60–130 %.

2.3.4. FC-72 on copper substrates

Fig. 10 compares the boiling curve for saturated boiling of FC-72 on enhanced copper substrates from seven different studies, while Table 7 summarizes the CHF value and the enhancement factors. The adopted enhancement approaches are summarized as follows:

(i) Macro pin–fin structure versus sintered porous layer: Yu and Lu [36] fabricated rectangular pin–fin array using electric discharge machining. The best performing surface was the one with the largest heat transfer area. The enhancement factors in CHF and HTC were 5.4 and 4.9 respectively with CHF value of 0.97 MW/m^2 at 34 K superheat. Sarangi et al. [38,82,83] investigated heat transfer enhancement using sintered copper particles. They studied the effect of particle morphology [82] (spherical, irregular, dendritic shapes), particle diameter [83] and porosity [38]. In all studies, the coating thickness was four times the particle diameter. It was found by [82] that the particle morphology did not have significant effect on CHF. The HTC was nearly independent of heat flux for the spherical particles, while it increased to a peak value after which it decreased with heat flux for the
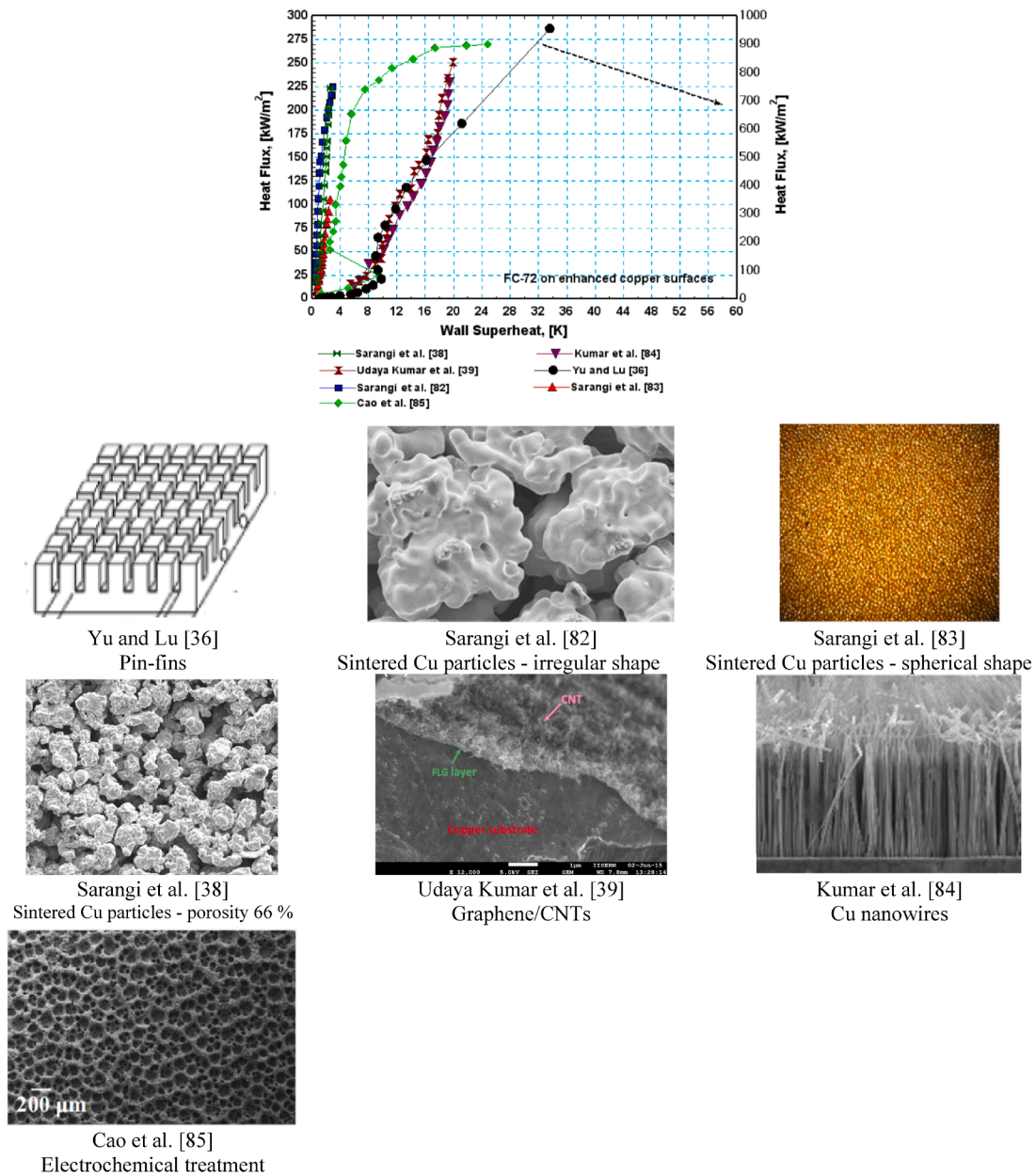
Fig. 10. Saturated boiling of FC-72 on enhanced copper surface.

irregular and dendrite shape particles. The decrease in HTC after a certain intermediate heat flux value was attributed to the trap of vapour inside the structure due to the smaller pore size. The surface with irregular shape particles exhibited the highest HTC with enhancement factors in CHF and HTC of 2 and 36.1, respectively with CHF value 0.225 MW/m^2 at 2.9 K superheat. The enhancement was attributed by [82] to the smaller pore size and tortuous rough structure of the irregular particles, which increased number of active nucleation sites and surface area. Regarding the effect of particle diameter, Sarangi et al. [83] found that the surface with sintered copper particles of size 45 – 53 μm exhibited the highest CHF and HTC and the enhancement factors in CHF and HTC were 0.95 and 11.4, respectively with CHF value of 0.105 MW/m^2 and 2.6 K superheat. Sarangi et al. [38] reported on the effect of porosity stating that a surface with irregular shape particles of porosity 66 % exhibited the best heat transfer performance. The enhancement factors in CHF and HTC are 2 and 23.8, respectively with CHF value found to be 0.224

MW/m^2 at 2.6 K superheat. It can be concluded that the sintered copper particles could achieve CHF of 0.22 MW/m^2 (100 % enhancement) with significant enhancements in the HTC (3510 %). It is interesting to note that this CHF value is nearly similar to that reported early in the previous section for saturated boiling of FC-72 on silicon substrates, although the substrate material and surface structure were different. The huge CHF value, 0.97 MW/m^2 reported by Yu and Lu [36] seems to be arising from the large surface area with the macro-pin–fin structure.

(ii) Surface coating: Udaya Kumar et al. [39,84] coated the surface either with copper or silver nanowires [39] and graphene/CNTs [84]. It was found by [39] that the effect of nanowire material was insignificant. The enhancement factors in CHF and HTC were 1.36, and 2.6 with CHF value of 0.229 MW/m^2 at 19.5 K super-heat. Changing the coating to hybrid graphene/CNTs, Udaya Kumar et al. [84] found that the enhancement factors in CHF and HTC were 1.4 and 2.6 with CHF value of 0.25 MW/m^2 at 20 K superheat. Cao et al. [85] tested a porous structure created by

Table 7
Boiling performance of FC-72 on copper substrates.

Author	Surface microstructure and preparation	CHF, [MW/m^2]	Enhancement Factors, [–]		ΔT_{CHF}[K]
			HTC	CHF	
Yu and Lu [36]	Rectangular pin–fin array of height 0.5–4 mm, pitch 0.5–2 mm and fin width 1 mm	Fins of height 4 mm and pitch 0.5 mm 0.96	4.9	5.4	33.6
Sarangi et al. [82]	Sintered copper particles of different morphology (spherical, irregular and dendritic)–particle diameter 90–106 μm and thickness 360–424 μm	Particles of irregular shape 0.225	36.1	2	2.9
Sarangi et al. [83]	Sintered copper particles – effect of particle diameter 45–1000 μm and compared between sintered and free particles sitting on the surface	Particle size 45–53 μm 0.11	11.4	0.95	2.6
Sarangi et al. [38]	Sintered copper particles of diameter 90–106 μm of spherical and irregular shape – effect of porosity 40–80 %	Irregular shape with porosity 66 % 0.224	23.8	2	2.6
Udaya Kumar [39]	Surface coated with metal nanowires (Cu versus Ag) with fixed wire diameter 0.2 μm, height 19–25 μm and pitch 260, 320, 360 μm.	Nanowire pitch 360 μm–no effect for wire material 0.23	2.6	136	19.5
Udaya Kumar [84]	Surface coated with hybrid graphene-carbon nanotube coating	Graphene/carbon nanotube coating 0.25	2.6	1.4	20
Cao et al. [85]	Surface enhanced with porous structure created by electrochemical deposition (porosity 0–60.8 %, Ra = 0.09–17 μm)	The surface with the highest Ra = 17 μm 0.27	6.73	1.54	25

electrochemical deposition technique that resulted in surfaces with Ra value in the range of 0.09 – 17 μm and porosity up to 60.8 %. It was observed that the boiling curve shifts to the left with increasing surface roughness. Thus, the enhancement factors for the rough surface (Ra = 17 μm) were 1.54 and 6.73 in CHF and HTC, respectively compared to the plain surface with CHF value of 0.27 MW/m^2 at 25 K superheat.

It can be concluded, from these studies and from section 4.3.3 for FC-72 on silicon substrates, that the CHF value of FC-72 did not change significantly with the surface microstructure and substrate material. It was in the range 0.25 – 0.3 MW/m^2 for silicon and copper. The highest enhancements in HTC were achieved with porous structures, e.g. 3510 % in case of sintered copper particles and 573 % in case of electrochemical treatment.

3. Discussion

There are large number of research papers on heat transfer enhancement using surface modifications. The review in this paper presented studies for two fluids – water and FC-72 – and two materials – silicon and copper - in order to help elucidate the enhancement mechanism(s) and quantify the changes in the heat transfer rates and critical heat flux. The following paragraphs summarizes our observations.

There is a need for a standard definition to what is called a "smooth surface" which was considered as the reference surface in each study. Indeed, there is a wide scatter in the microstructure of the smooth surface from one study to another, which results in different CHF values. For example, the reference surface by Wu et al. [24] achieved 1.7 MW/m^2 for water on copper while Khan et al. [5] reported only 0.77 MW/m^2.

Thus, inferring the performance of enhanced surfaces using percent enhancement (or enhancement factor) will be misleading to conclude on the best microstructure for a boiling surface, unless there is an agreed, unified definition to the "smooth surface".

The criterion of inferring the CHF should be unified among researchers because it is subjective. Most researchers detect the CHF from the sudden rise in surface temperature. However, they did not agree on the extent of this temperature rise. Some researchers allow sudden temperature rise of 10 K, some others allow 20 K and other researchers may allow even much higher values. Additionally, in some cases, researcher force the experimental system to reach very high superheat values. For example, Ahn et al. [79] recorded the CHF at 86 K superheat for water while Zhang et al. [67] recorded CHF at 250 K superheat. This will result in a wide scatter in the performance of existing CHF predictive equations, in addition to being impractical.

Although pool boiling test rigs are nearly the same in all studies, there is a need for validating the experimental system. Some researchers tested thin copper discs (about 3 mm thick) with thin film heater attached to the back side. In this case, the heat flux was calculated from the effective power divided by area. Another group of researchers used copper block (one piece) of which the top surface was the boiling surface and the heat flux was calculated from the measured temperature gradient. A third group designed the test section as a thin disk attached to the top surface of a big copper block which has vertical thermocouples for heat flux measurements. In this case, some people ignored the thermal contact resistance, while some others considered this resistance. To avoid these issues, system validation is required. Many researchers did not report on system validation while some others validated the system using the Rohsenow [57] pool boiling correlation for a smooth surface. In some cases, the results did not agree with the correlation and the reason could be either the surface microstructure or the experimental setup. Because pool boiling correlations are affected significantly by the surface microstructure, the present authors recommend that validation should be conducted in single-phase, using single phase natural convection correlations.

Nearly, in all studies, the structured surfaces were fabricated in a random manner. In other words, the recommended heterogeneous nucleation theories were not adopted in the surface design. Also, the test surfaces were analyzed through the SEM images or roughness profile without specifying the cavity geometrical parameters (depth and width). In most cases, the average roughness (Ra) was used as a surface parameter, which is not related directly to the nucleation theories. In fact, there is a need for the research community to agree on the definition of a cavity. The heterogeneous nucleation theories are referring to conical cavities (conical crevices). Surface protrusions, surface scratches and valleys (very common on enhanced surfaces) are not of that shape, i. e. not conical. There is also the need to consider and define cavities and their shapes in porous structures. This also poses the question of the relative importance in pool boiling of roughness parameters or surface porosity.

The analysis above and the results of past work clearly indicates that surfaces with uniform hydrophobic/superhydrophobic surfaces are not recommended as boiling heat transfer surfaces due to the extremely low CHF. In hydrophobic surfaces, boiling starts at extremely low superheat which enhances the HTC significantly at very low heat fluxes. However, with increasing heat flux the slope of the boiling curve decreases significantly due to the fact that bubble size is extremely larger in hydrophobic surfaces with extremely large dry contact area, i.e. no liquid wetting underneath the bubble. This triggers the CHF early.

The research community agrees on the fact that any change in the surface microstructure may enhance the heat transfer rate and CHF by a certain amount. However, the discrepancy occurs when researcher try to quantify the enhancement. Some researchers use the word "superior" to report enhancements in the order of 15 – 30 %. Therefore, the research community should agree on the ranking criterion of the performance of enhanced surfaces. The current authors suggest three classes for ranking

the enhancement techniques:

Class A. The enhancement techniques achieve enhancement factors less than or similar to the machined rough surfaces (intrinsic roughness due to machining). In this case, these enhancement techniques will not be economic and should not be recommended for industry.

Class B. The enhancement factors are greater than those of the roughened surfaces and less than 5.

Class C. The enhancement factors are greater than 5 and, in that case, they may be called "superior surfaces".

Additionally, the present authors recommend a standard method and specifications for a rough surface to be agreed as a benchmark in this ranking criterion.

In this study we have examined two fluids representing extremely high wetting (low surface tension) and less wetting (high surface tension), namely FC-72 and water on two different surfaces, i.e. silicon and copper, covering experimental and industrially relevant past work. For saturated boiling of water on roughened copper surfaces, the enhancement factors of CHF and HTC ranged from 1.1 to 2 and 1.7 to 2.8, respectively. The highest CHF for saturated boiling of water on roughened copper and aluminum surfaces were 1.7 and 2.15 MW/m^2, respectively. For dielectric liquids (FC-72, FC-77, HFE-7000, HFE-7100) the enhancement values ranged from 1.4 to 1.5 and 2.2 to 3.9, respectively for saturated boiling on roughened metallic surfaces (brass, copper and aluminum). The CHF value was about 0.3 MW/m^2 for HFEs and about 0.2 MW/m^2 for FCs.

For saturated boiling of water on plain silicon substrates, the CHF is about 1 MW/m^2 while it is about 0.16 MW/m^2 for FC-72. For enhanced silicon substrates, the enhancement factors in CHF and HTC ranged from 1.15 to 2.7 and 1.6 to 3.7, respectively. The highest enhancement factors were achieved with the structure suggested by Yao et al. [10] which is parallel microchannels with silicon nanowires on the channel walls. The second-best surface structure was the one suggested by Liu et al. [8] which is micro-pins at selective areas and fully coated with SiO$_2$. The third best surface was the one suggested by Kwak et al. [11], parallel channels coated with SiO$_2$. For saturated boiling of FC-72 on enhanced silicon substrates, the enhancement factors of CHF and HTC were 1.5–1.9 and 2.5–4.6, respectively. The CHF ranged from 0.17 to 0.3 MW/m^2. The best performing surfaces were the one proposed by Ujereh et al. [31], which was a surface coated with multi-walls carbon nanotubes, followed by the surface treated by femtosecond laser suggested by Liu et al. [32]. For sub-cooled boiling of FC-72 on enhanced silicon substrates, the enhancement factors of CHF and HTC ranged from 2 to 2.3 and 1.6 to 5.9, respectively. The best performing structure was the one suggested by Duan et al. [34] which was cylindrical micro-pin-fins of a mixed fin diameter. The second-best surface was the one proposed by Zhou et al. [33] which was a square micro-pin-fins. All studied agreed on that the CHF value was about 0.55 MW/m2 for sub-cooled boiling of FC-72 on silicon substrates.

For saturated boiling of water on enhanced copper substrates, the best performing structure was the one recommended by Jaikumar and Kandlikar [14], which achieved CHF value of 4.2 MW/m^2 at 2 K superheat. This microstructure consisted of parallel microchannels with sintered copper particles on the channel walls. The above CHF value was also achieved by Zhang et al. [67] using sintered copper plate on top of parallel microchannels and Wu et al. [24] using parallel channels with holes in the separating walls fabricated by selective laser melting. However, the wall superheat was significantly higher (about 25 K) compared to Jaikumar and Kandlikar. For saturated boiling of FC-72 on enhanced copper surfaces, the enhancement factors in CHF and HTC ranged from 1 to 5.4 and 2.6 to 36, respectively. The best performing surface was the one with pin-fins cut by WEDM and reported by Yu and Lu [36]. The CHF value with this structure reached about 1 MW/m^2 at 34 K superheat. In all other studies the CHF ranged from 0.1 to 0.27 MW/m^2 and the lowest wall superheat (highest enhancements in HTC) occurred with the sintered copper layer in the studies by Sarangi et al. [38,82,83].

This study revealed that the different enhancement mechanisms, assumed (not validated) by researchers, can be classified as follows, see Fig. 11:

1. The increase of the number of active nucleation sites induced by the modified surface texture (Fig. 11b).
2. The enhancement of capillary wicking induced by the porous microstructure, as seen in Fig. 11c.
3. Segregation of the liquid and vapour pathways. This was conducted by: (a) mixed wettability, which enhances the liquid supply to the surface and thus increases the CHF. This was carried out by selectively coating a hydrophilic surface with hydrophobic spots as illustrated in Fig. 11d. In this approach, bubbles nucleate at low wall superheat at the hydrophobic spots and suppresses nucleation from the surrounding hydrophilic areas due to the local lateral cooling induced by nucleation at the hydrophobic spots. Accordingly, the triple contact line did not spread beyond the hydrophobic spots and thus lateral bubble coalescence diminishes, which creates space for liquid to replenish the surface. With this pattern, the bubble size can be controlled. (b) modulated porous structure as seen in Fig. 11e and 11f. In Fig. 11e, the surface is coated with a porous layer on top of which vertical mountain shapes are created. The bubbles nucleate from the flat porous areas while the liquid replenishment occurs through the vertical porous elements through capillary wicking. In Fig. 11f, micro-pin-fins were created at selective areas on the surface. In this approach, bubbles nucleate on top of the fins and the capillary liquid supply occurs through the un-finned areas. (c) attachment of plastic fixture with a certain pattern (Fig. 11g). The walls of the fixture are porous and because it has low thermal conductivity, nucleation is limited to the metallic surface and liquid replenishment occurs through the porous walls. (d) parallel microchannels with coated fins (Fig. 11*h*). In this mechanism, bubbles nucleate from the porous fin tip and the liquid falls down and impinge the channel bottom resulting in enhancements in heat transfer rate.
4. Enhancement in surface wettability and surface area. It is commonly agreed that hydrophobic surfaces have very low CHF but very high heat transfer rate at low heat fluxes. Increasing the surface wettability increases the CHF.

Conclusions

In this paper we reviewed and discussed the performance of water and FC-72 on smooth, rough and enhanced copper and silicon substrates. The major conclusions of this work are given below:

1. The mechanism of increasing the slope of the boiling curve, for small size boiling surfaces (about 10 × 10 mm), depends on the type of fluid. Nearly, all researchers attributed it to the increased number of active nucleation sites, which may be correct only for dielectric liquids with small bubble departure diameter. For liquids with large bubble departure diameter such as water, few nucleation sites can be active and cover the whole surface. The large bubble size could suppress nucleation in the region of bubble influence. Thus, the increase in the slope is due to the increase in the evaporation rate with the increase in heat flux. Thus, water may not be affected by the surface microstructure, except only at boiling incipience (very low heat fluxes), especially when the size of boiling surface is small. This point needs further experimental studies for validation.
2. There is a large discrepancy among researchers on the performance of the reference surface although the fluid and substrate material were the same. This may affect the enhancement factors calculated for the enhanced surfaces.
3. The current authors recommend that the research community should adopt a standard definition to what is called a "smooth surface" and unify the method of surface preparation, in order to assess properly and record the enhancement in the HTC and the CHF. Additionally, it
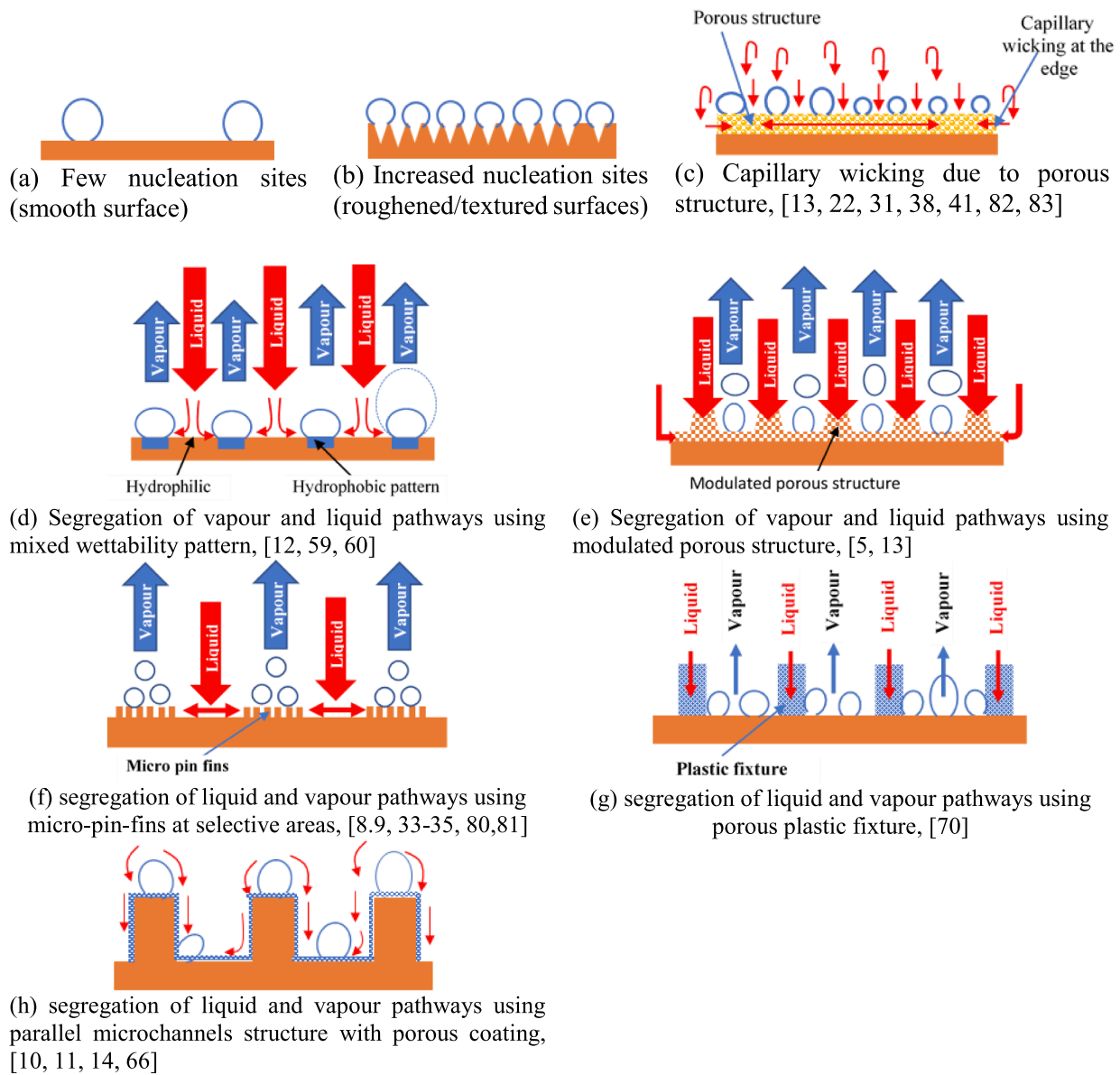
(a) Few nucleation sites (smooth surface)

(b) Increased nucleation sites (roughened/textured surfaces)

(c) Capillary wicking due to porous structure, [13, 22, 31, 38, 41, 82, 83]

(d) Segregation of vapour and liquid pathways using mixed wettability pattern, [12, 59, 60]

(e) Segregation of vapour and liquid pathways using modulated porous structure, [5, 13]

(f) segregation of liquid and vapour pathways using micro-pin-fins at selective areas, [8.9, 33-35, 80,81]

(g) segregation of liquid and vapour pathways using porous plastic fixture, [70]

(h) segregation of liquid and vapour pathways using parallel microchannels structure with porous coating, [10, 11, 14, 66]

Fig. 11. Heat transfer enhancement mechanisms suggest by researchers in the literature.

is better to test two reference surfaces (smooth and rough, the latter made of a cheap, readily available manufacturing method) in order to conclude on the performance of enhanced surfaces. Applying this criterion, one can see that several enhancement techniques produce surfaces that perform similar or even worse than the intrinsic rough surfaces. This could help refine the huge number of surfaces prepared by some complex and expensive techniques.

4. Saturated boiling of water on copper surfaces roughened by sandpaper achieved 100 % enhancement in the CHF and 175 % enhancement in the HTC with CHF value up to 1.7 MW/m^2. Dielectric liquids achieved 0.2–0.3 MW/m^2. It is worth mentioning that surface aging and oxidation were not studied in literature and these enhancement values could be affected by surface oxidation.

5. Saturated boiling of water on silicon substrates enhanced with coated parallel microchannels achieved a CHF value of 2.5 MW/m^2, while with copper substrates the highest achieved CHF value was 4.2 MW/m^2 for parallel microchannels coated with sintered copper particles. Modulated sintered copper particles achieved CHF up to 3.8 MW/m^2 while nanocoating achieved up to 2.9 MW/m^2.

6. The CHF value of FC-72 on enhanced copper and silicon substrate was about 0.3 MW/m^2 for saturated boiling and 0.5 MW/m^2 for subcooled boiling.

Declaration of Competing Interest

The authors declare that they have no known competing financial interests or personal relationships that could have appeared to influence the work reported in this paper.

References

[1] M.M. Mahmoud, T.G. Karayiannis, Pool boiling review: Part I - Fundamentals of boiling and relation to surface design, Therm. Sci. Eng. Prog. (2021), https://doi.org/10.1016/j.tsep.2021.101024.

[2] D.A. Reay, Heat transfer enhancement – a review of techniques and their possible impact on energy efficiency in the UK, Heat Recovery Syst. CHP 11 (1) (1991) 1–40.

[3] J.R. McDonough, A perspective on the current and future roles of additive manufacturing in process engineering, with an emphasis on heat transfer, Thermal Sci. Eng. Progress 19 (2020) 100594.

[4] N. Sezer, S.A. Khan, M. Koç, Koç, Amelioration of the pool boiling heat transfer performance via self-assembling of 3D porous graphene/carbon nanotube hybrid film over the heating surface, Int. J. Heat Mass Transfer 145 (2019) 118732.

[5] S.A. Khan, N. Sezer, M. Koç, Design, fabrication and nucleate pool boiling heat transfer performance of hybrid micro-nano scale 2D modulated porous surfaces, Appl. Therm. Eng. 153 (2019) 168–180.

[6] A. Sankaran, W. Zhang, A.L. Yarin, Pool boiling in deep and shallow vessels and the effect of surface nanotexture and self-rewetting, Int. J. Heat Mass Transfer 127 (2018) 857–866.

[7] J.M. Kim, B.T. Kong, H.-B.-R. Lee, S. Wongwises, H.S. Ahn, Effect of h-BN coating on nucleate boiling heat transfer performance in pool boiling, Exp. Thermal Fluid Sci. 98 (2018) 12–19.

[8] Y. Liu, M.-C. Lu, D. Xu, The suppression effect of easy-to-activate nucleation sites of the critical heat flux in pool boiling, Int. J. Thermal Sci. 129 (2018) 231–237.

[9] Y. Liu, J. Tang, L. Li, Y.N. Shek, D. Xu, Design of Cassie-wetting nucleation sites in pool boiling, Int. J. Heat Mass Transfer 132 (2019) 25–33.

[10] Z. Yao, Y.-W. Lu, S. G. Kandlikar, Pool boiling heat transfer enhancement through nanostructures on silicon microchannels, J. Nanotechnol. Eng. Med., 3, 031002-1 – 031002-8, 2012.

[11] H.J. Kwak, J.H. Kim, B.-S. Myung, M.H. Kim, D.E. Kim, Behavior of pool boiling heat transfer and critical heat flux on high aspect ratio microchannels, Int. J. Thermal Sci. 125 (2018) 111–120.

[12] D.Y. Lim, I.C. Bang, Controlled bubble departure diameter on biphilic surfaces for enhanced pool boiling heat transfer performance, Int. J. Heat Mass Transfer 150 (2020) 119360.

[13] R.P. Rioux, E.C. Nolan, C.H. Li, A systematic study of pool boiling heat transfer on structured porous surfaces: from nanoscale through microscale to macroscrale, AIP Adv. 4 (2014), 117133.

[14] A. Jaikumar, S.G. Kandlikar, Ultra-pool boiling performance and effect of channel width with selectively coated open microchannels, Int. J. Heat Mass Transfer 95 (2016) 795–805.

[15] D. Deng, W. Wan, J. Feng, Q. Huang, Y. Qin, Y. Xie, Comparative experimental study on pool boiling performance of porous coating and solid structures with reentrant channels, Appl. Therm. Eng. 107 (2016) 420–430.

[16] R.R. Souza, L.L. Manetti, I.S. Kiyomura, E.M. Cardoso, Liquid/surface interaction during pool boiling of DI-water on nanocoated heating surface, J. Brazil. Soc. Mech. Sci. Eng. 40 (2018) 514.

[17] V. Kumar, S.S. Gajghate, U. Nath, A. Pal, S. Bhaumik, S. Das, Experimental studies on nucleate pool boiling heat transfer enhancement for composite nano-structure coated copper heating surface, J. Phys. Conf. Series 1240 (2019) 012055.

[18] A.M. Rishi, S.G. Kandlikar, A. Gupta, Improved wettability of graphene nanoplatelets (GNP)/copper porous coating for dramatic improvements in pool boiling heat transfer, Int. J. Heat Mass Transfer 132 (2019) 462–472.

[19] A.M. Gheitaghy, H. Saffari, G.Q. Zhang, Effect of nanostructured microporous surfaces on pool boiling augmentation, Heat Transfer Eng. 40 (9-10) (2019) 762–771.

[20] G. Chen, C.H. Li, Combined effects of liquid wicking and hydrodynamic instability on pool boiling critical heat flux by two tier-copper structures of nanowires and microgrooves, Int. J. Heat Mass Transfer 129 (2019) 1222–1231.

[21] S.K. Gupta, R.D. Misra, Experimental study of pool boiling heat transfer on copper surfaces with Cu-Al2O3 nanocomposite coatings, Int. Commun. Heat Mass Transfer 97 (2018) 47–55.

[22] R.J. MacNamara, T.L. Lupton, R. Lupoi, A.J. Robinson, Enhanced nucleate pool boiling on copper-diamonds textured surfaces, Appl. Therm. Eng. 162 (2019), 114145.

[23] C. Kruse, A. Tsubaki, C. Zuhlke, D. Alexander, M. Anderson, E. Peng, J. Shield, S. Ndao, G. Gogos, Influence of copper oxide on femtosecond laser surface processed copper pool boiling heat transfer surfaces, J. Heat Transfer, 141, 0501503-1 – 05051503-9, 2019.

[24] T. Wu, P. S. Lee, J. Mathew, C-N. Sun, B. L. Aw, Pool boiling heat transfer enhancement with porous fin arrays manufactured by selective laser melting, 18th IEEE ITHERM Conf., 2019.

[25] L. Mao, W. Zhou, X. Hu, Y. He, G. Zhang, L. Zhang, R. Fu, Pool boiling performance and bubble dynamics on graphene oxide nanocoating surface, Int. J. Thermal Sci., 147, 106154, 2020.

[26] J. Kim, S. Jun, J. Lee, J. Godinez, S. M. You, Effect of surface roughness on pool boiling heat transfer of water on superhydrophilic aluminium surface, J. Heat Transfer, vol. 139, 101501-1 – 101501-9, 2017.

[27] A. Hayes, P.A. Raghupathi, T.S. Emery, S.G. Kandlikar, Regulating flow of vapour to enhance pool boiling, Appl. Therm. Eng. 149 (2019) 1044–1051.

[28] J.C. Godinez, D. Fadda, J. Lee, S.M. You, Enhancement of pool boiling heat transfer in water on aluminium surface with high temperature conductive microporous coating, Int. J. Heat Mass Transfer 132 (2019) 772–781.

[29] C.M. Kruse, T. Anderson, C. Wilson, C. Zuhlke, D. Alexander, G. Gogos, S. Ndao, Enhanced pool boiling heat transfer and critical heat flux on femtosecond laser processed stainless steel surfaces, Int. J. Heat Mass Transfer 82 (2015) 109–116.

[30] C. Zhang, L.i. Zhang, H. Xu, P. Li, B. Qian, Performance of pool boiling with 3D grid structure manufactured by selective laser melting technique, Int. J. Heat Mass Transfer 128 (2019) 570–580.

[31] S. Ujereh, T. Fisher, I. Mudawar, Effects of carbon nanotube arrays on nucleate pool boiling, Int. J. Heat Mass Transfer 50 (2007) 4023–4038.

[32] B. Liu, J. Liu, Y. Zhang, J. Wei, W. Wang, Experimental and theoretical study of pool boiling heat transfer and its CHF mechanism on femtosecond laser processed surfaces, Int. J. Heat Mass Transfer 132 (2019) 259–270.

[33] J. Zhou, B. Qi, J. Wei, Critical heat flux on heterogeneous fractal surfaces with micro-pin-fins in pool boiling part I: the effects of distribution and subcooling, Int. J. Heat Mass Transfer 136 (2019) 1338–1348.

[34] L. Duan, B. Liu, B. Qi, Y. Zhang, J. Wei, Pool boiling heat transfer on silicon chips with non-uniform micro-pillars, Int. J. Heat Mass Transfer 151 (2020) 119456.

[35] Z. Lei, B. Liu, P. Xu, Y. Zhang, J. Wei, The pool boiling heat transfer and critical vapour column coalescence mechanism of block-divided microstructured surfaces, Int. J. Heat Mass Transfer 150 (2020), 119362.

[36] C.K. Yu, D.C. Lu, T.C. Cheng, Pool boiling heat transfer on artificial micro-cavity surfaces in dielectric fluid FC-72, J. Micromech. Microeng. 16 (2006) 2092–2099.

[37] U.G. Kumar, S. Suresh, M.R. Thansekhar, D.P. Babu, Effect of diameter of metal nanowires on pool boiling heat transfer with FC-72, Appl. Surf. Sci. 423 (2017) 509–520.

[38] S. Sarangi, J.A. Weibel, S.V. Garimella, Quantitative evaluation of the dependence of pool boiling heat transfer enhancement on sintered particle coating characteristics, J. Heat Transfer 139 (2) (2017) 4034901.

[39] G. Udaya Kumar, S. Suresh, M.R. Thansekhar, D. Halpati, Role of inter-nanowire distance in metal nanowires on pool boiling heat transfer characteristics, J. Colloid Interface Sci. 532 (2018) 218–230.

[40] M. Zimmermann, M. Heinz, A. Sielaff, T. Gambaryan-Roisman, P. Stephan, Influence of system pressure on pool boiling regimes on a microstructured surface compared to a smooth surface, Exp. Heat Transfer 33 (4) (2020) 318–334.

[41] J. Kim, J. Yoem, D. Kong, H. Lee, S.-M. Kim, Analysis of the enhancing mechanism in pool boiling heat transfer through wetting speed for rough aluminium surfaces with FC-72, Int. J. Heat Mass Transfer 150 (2020), 119325.

[42] J.P. McHale, S.V. Garimella, T.S. Fisher, G.A. Powell, Pool boiling performance comparison of smooth and sintered copper surfaces with and without carbon nanotubes, Nanoscale Microscale Thermophys. Eng. 15 (3) (2011) 133–150.

[43] Z. Wu, Z. Cao, B. Sundén, Saturated pool boiling heat transfer of acetone and HFE-7200 on modified surfaces by electrophoretic and electrochemical deposition, Appl. Energy 249 (2019) 286–299.

[44] Z. Cao, Z. Wu, A.-D. Pham, B. Sundén, Electrophoretic deposition surfaces to enhance HFE-7200 pool boiling heat transfer and critical heat flux, Int. J. Thermal Sci. 146 (2019) 106107.

[45] B. Doran, B. Zhang, A. Walker, P. KC, W.J. Meng, A.L. Moore, Experimental determination of the role of increased surface area in pool boiling from nanostructured surfaces, Exp. Thermal Fluid Sci. 111 (2020) 109956.

[46] C. Kruse, M. Lucis, J. Shield, T. Anderson, C. Zuhike, D. Alexander, G. Gogos, S, Ndao, Effects of femtosecond laser surface processed nanoparticle layers on pool boiling heat transfer performance, J. Thermal Sci. Eng. Appl. 10(3), 031009, 2018.

[47] J. Kim, S. Jun, R. Laksnarain, S.M. You, Effect of surface roughness on pool boiling heat transfer at a heated surface having moderate wettability, Int. J. Heat Mass Transfer 101 (2016) 992–1002.

[48] J.S. Kim, A. Girard, S. Jun, J. Lee, S.M. You, Effect of surface roughness on pool boiling heat transfer of water on hydrophobic surfaces, Int. J. Heat Mass Transfer 118 (2018) 802–811.

[49] A. Walunj, A. Sathyabhama, Influence of surface roughness on pool boiling heat transfer, IOP Conf, Series: Mater. Sci. Eng. 402 (2018), 012081.

[50] V.V. Nirgude, S.K. Sahu, Enhancement in nucleate pool boiling heat transfer on nano-second laser processed copper surfaces, Exp. Heat Transfer 32 (6) (2019) 566–583.

[51] S. Fan, L. Jiao, K. Wang, F. Duan, Pool boiling heat transfer of saturated water on rough surfaces with the effect of roughening techniques, Int. J. Heat Mass Transfer 159 (2020) 120054.

[52] D. Mani, S. Sivan, H. M. Ali, U.K. Ganesan, Investigation to improve the pool boiling heat transfer characteristics using laser-textured copper grooved surfaces, Int. J. Photoenergy, 3846157, 2020.

[53] B.J. Jones, J.P. McHale, S.V. Garimella, The influence of surface roughness on nucleate pool boiling heat transfer, J. Heat Transfer 131 (12) (2009) 1–14.

[54] P. Fariñas Alvariño, M.L. Sánchez Simón, M. dos Santos Guzella, J.M. Amado Paz, J.M. Sáiz Jabardo, L. Cabezas Gómez, Experimental investigation of the CHF of HFE-7100 under pool boiling conditions on differently roughened surfaces, Int. J. Heat Mass Transfer 139 (2019) 269–279.

[55] M.S. El-Genk, M. Pourghasemi, Experimental investigation of saturation boiling of HFE-7100 dielectric liquid on rough copper surfaces, Thermal Sci. Eng. Progr. 15 (2020), 100428.

[56] W. Fritz, Berech des maximal volume von dampf blasen, Phys. Z. 36 (1935) 379–388.

[57] W.M. Rohsenow, A Method of Correlating Heat Transfer Data for Surface Boiling of Liquids, Technical Report No 5, Office of the Naval Research, Massachusetts Inst Of Technology, 1951.

[58] N. Mohammadi, D. Fadda, C.K. Choi, J. Lee, S.M. You, Effects of surface wettability on pool boiling of water using super-polished silicon surfaces, Int. J. Heat Mass Transfer 127 (2018) 1128–1137.

[59] A.R. Betz, J. Jenkins, C.-J. Kim, D. Attinger, Boiling heat transfer on superhydrophilic, superhydrophobic, and superbiphilic surfaces, Int. J. Heat Mass Transfer 57 (2) (2013) 733–741.

[60] M.M. Rahman, M. McCarthy, Effect of length scales on the boiling enhancement of structured copper surfaces, J. Heat Transfer 139 (11) (2017) 111508.

[61] D. Cooke, S.G. Kandlikar, Effect of open microchannel geometry on pool boiling enhancement, Int. J. Heat Mass Transfer 55 (4) (2012) 1004–1013.

[62] G. Chen, M. Jia, S. Zhang, Y. Tang, Z. Wan, Pool boiling enhancement of novel interconnected microchannels with reentrant cavities for high power electronics cooling, Int. J. Heat Mass Transfer 156 (2020) 119836.

[63] R.K. Gouda, M. Pathak, M.K. Khan, Pool boiling heat transfer enhancement with segmented finned microchannels structured surface, Int. J. Heat Mass Transfer 127 (2018) 39–50.

[64] F. Hai, W. Zhu, S. Liang, X. Yang, Y. Deng, Enhanced pool boiling performance of microchannel patterned surface with extremely low wall superheat through capillary feeding of liquid, Nanoscale Microscale Thermophys. Eng. 24 (2) (2020) 66–79.

[65] H. Saffari, H. Fathalizadeh, H. Moghadasi, S. Alipour, S.M. Hosseinalipour, Experimental study of pool boiling enhancement for surface structuring with inclined intersected mesochannels using WEDM method on copper surfaces, J. Thermal Anal. Calorimetry 139 (2020) 1849–1861.

[66] A. Jaikumar, S.G. Kandlikar, Enhanced pool boiling heat transfer mechanisms for selectively sintered open microchannels, Int. J. Heat Mass Transfer 88 (2015) 652–661.

[67] K. Zhang, L. Bai, G. Lin, H. Jin, D. Wen, Experimental study on pool boiling in a porous artery structure, Appl. Therm. Eng. 149 (2019) 377–384.

[68] G. Pi, D. Deng, L. Chen, X. Xu, C. Zhao, Pool boiling performance of 3D-printed reentrant microchannels structures, Int. J. Heat Mass Transfer 156 (2020) 119920.

[69] H. Cho, J. Godinez, J.S. Han, D. Fadda, S.M. You, J. Lee, S.J. Park, Fabrication of micro-patterned surface for pool boiling enhancement by using powder injection molding process, Materials 12 (3) (2019) 507.

[70] A. Elkholy, R. Kemperes, Enhancement of pool boiling heat transfer using 3D-printed polymer fixture, Exp. Therm Fluid Sci. 114 (2020), 110056.

[71] S. Mori, S. Mt Aznam, K. Okuyama, Enhancement of the critical heat flux in saturated pool boiling of water by nanoparticle-coating and a honeycomb porous plate, Int. J. Heat Mass Transfer 80 (2015) 1–6.

[72] S. Jun, H. Wi, A. Gurung, M. Amaya, S. M. You, Pool boiling heat transfer enhancement of water using brazed copper microporous coating, Proceedings of the ASME 2015 Int. Mech. Eng. Congress and Exposition IMECE2015, November 13 – 19, 2015, Houston, Texas.

[73] S.S. Gajghate, S. Barathula, S. Das, B.B. Saha, S. Bhaumik, Experimental investigation and optimization of pool boiling heat transfer enhancement over graphene-coated copper surface, J. Thermal Anal. Calorimetry 140 (3) (2020) 1393–1411.

[74] G. Patel, S.S. Gajghaty, A. Pal, U. Nath, S. Bhaumik, S. Das, Experimental investigation on nucleate boiling heat transfer enhancement for nanostructured copper oxide coated heating surface, J. of Phys.: Conf. Series 1240 (2019), 012093.

[75] H.S. Jo, T.G. Kim, J.-G. Lee, M.-W. Kim, H.G. Park, S.C. James, J. Choi, S.S. Yoon, Supersonically sprayed nanotextured surfaces with silver nanowires for enhanced pool boiling, Int. J. Heat Mass Transfer 123 (2018) 397–406.

[76] S.K. Gupta, R.D. Misra, Effect of two-step electrodeposited Cu-TiO2 nanocomposite coating on pool boiling heat transfer performance, J. Thermal Anal. Calorimetry 136 (2019) 1781–1793.

[77] D.-C. Mo, S. Yang, J.-L. Luo, Y.-Q. Wang, S.-S. Lyu, Enhanced pool boiling performance of a porous honeycomb copper surface with radial diameter gradient, Int. J. Heat Mass Transfer 157 (2020) 119867.

[78] H.S. Ahn, V. Sathyamurthi, D. Banerjee, Pool boiling experiments on a nano-structured surface, IEEE Trans. Compon. Packag. Technol. 32 (1) (2009) 156–165.

[79] B. Liu, J. Liu, J. Zhou, B. Yuan, Y. Zhang, J. Wei, W. Wang, Experimental study of subcooled boiling pool heat transfer and its "hook back" phenomenon on micro/nanostructured surfaces, Int. Commun. Heat Mass Transfer 100 (2019) 73–82.

[80] X. Kong, Y. Zhang, J. Wei, Experimental study of pool boiling heat transfer on novel bistructured surfaces based on micro-pin-fined structure, Exp. Therm. And Fluid Sci. 91 (2018) 9–19.

[81] Z. Cao, B. Liu, C. Preger, Z. Wu, Y. Zhang, X. Wang, M.E. Messing, K. Deppert, J. Wei, B. Sundén, Pool boiling heat transfer of FC-72 on pin-fin silicon surfaces with nanoparticle deposition, Int. J. Heat Mass Transfer 126 (2018) 1019–1033.

[82] S. Sarangi, J.A. Weibel, S. V. Garimella, Effect of particle morphology on pool boiling from surfaces coated with sintered particles, Proceedings of the ASME 2015 Int. Mech. Eng. Congress and Exposition IMECE2015, November 13-19, 2015, Houston, Texas.

[83] S. Sarangi, J.A. Weibel, S.V. Garimella, Effect of particle size on surface coating enhancement of pool boiling heat transfer, Int. J. Heat Mass Transfer 81 (2015) 103–113.

[84] G. Udaya Kumar, K. Soni, S. Suresh, K. Ghosh, M.R. Thansekhar, P. Dinesh Babu, Modified surfaces using seamless graphene/carbon nanotubes based nanostructures for enhancing pool boiling heat transfer, Exp. Therm. Fluid Sci. 96 (2018) 493–506.

[85] Z. Cao, Z. Wu, B. Sundén, Heat transfer prediction and critical heat flux mechanism for pool boiling of NOVEC-649 on microporous copper surfaces, Int. J. Heat Mass Transfer 141 (2019) 818–834.

[86] D. Bonn, J. Egger, J. Indekeu, J. Meunier, E. Rolley, Wetting and spreading, Rev. Modern Phys. 181 (2009).